

# Aggregation of Charged Colloidal Particles

Nikolai I. Lebovka

**Abstract** This chapter reviews the recent progress in aggregation of colloidal particles with long-range interactions, including simple colloids and polyelectrolytes. The relevant interactions between colloidal particles, including Born repulsion, van der Waals, electrostatic, structural solvation, hydrophobic hydrodynamic interactions and attraction between like-charge colloids, charge nonuniformity, and adsorbed polymer, are analyzed. The main types of computer models used for simulation of cluster morphology and aggregation kinetics of the different interacting species (similarly and oppositely charged particles and polyelectrolytes) are reviewed. The main scaling laws for different aggregating kernels that describe diffusion-limited, reaction-limited, gelling, and retarded aggregations are also presented and analyzed.

**Keywords** Aggregation · Charged particles · Colloids · Kinetics · Morphology · Polyelectrolyte complex (PEC)

## Contents

1	Introduction .....	58
2	Interactions Between Colloidal Particles .....	59
2.1	van der Waals Interactions .....	60
2.2	Electrostatic Interactions .....	62
2.3	Born Repulsion .....	65
2.4	Structural Solvation Interactions .....	65
2.5	Hydrophobic Interactions .....	66
2.6	Effect of Polymers .....	66
2.7	Hydrodynamic Interactions .....	67

---

N.I. Lebovka (✉)

Institute of Biocolloidal Chemistry Named After F.D. Ovcharenko, NAS of Ukraine,  
42, blvr. Vernadskogo, 03142 Kiev, Ukraine  
e-mail: [lebovka@gmail.com](mailto:lebovka@gmail.com)

2.8	Interaction Between Colloidal Aggregates .....	68
3	Simulation of Cluster Morphology .....	68
3.1	Main Types of Computer Models .....	68
3.2	Similarly Charged Particles .....	69
3.3	Oppositely Charged Particles .....	76
3.4	Effect of Dipolar Interactions .....	78
4	Kinetics of Aggregation .....	78
4.1	Aggregation as a Second-Order Reaction .....	79
4.2	Population Balance Equations .....	81
4.3	Popular Kernels .....	82
4.4	Classification of Kernels .....	84
4.5	Dynamic Scaling .....	85
5	Conclusion .....	89
	References .....	90

## 1 Introduction

Polymeric nanoparticles are colloidal particles consisting of macromolecular compounds. Among these materials the polyelectrolyte complex (PEC) nanoparticles are of particular interest. These particles with integrated drugs, proteins, vaccines, or diagnostic agents can be used as carriers in different pharmaceutical and biomedical applications [1]. The benefits of their use include controlled drug release and limited toxicity. Moreover, water-soluble and biodegradable PEC nanoparticles may be used as drug delivery systems in humans [2, 3].

PEC nanoparticles are prepared by mixing of two oppositely charged polyanions and polycations. Formation of PEC nanoparticles is controlled by the structure of the polycation/polyanion components, concentration, mixing order, mixing ratio, ionic strength, pH, temperature, and other factors [4]. Key factors determining successful applications of PEC nanoparticles are related to good reproducibility of the formation process, monomodality, and the possibility of obtaining particles with determined and graded sizes.

The process of PEC nanoparticle formation usually includes the initial diffusion stage of mutual entanglement between polymers and formation of primary particles and the further stage of their aggregation and rearrangement of the already formed aggregates [2, 4]. The macroscopically homogeneous systems containing very small primary PEC nanoparticles (approximately 5–20 nm) were developed using special preparation techniques [5]. The process of aggregation of the primary PEC nanoparticles may result in formation of larger nanoparticles. As a result, a turbid colloidal, or two-phase system of supernatant liquid and precipitated PEC nanoparticles is formed [6]. Using of consecutive centrifugation and separation steps allows significant decrease in the polydispersity of the colloidal system, elimination of the primary PEC nanoparticles, and, finally, prevailing of the secondary nanoparticles with radii of about 100–200 nm in dispersion [4]. The secondary PEC nanoparticles have many particular advantages for applications in

biomedicine [7]. Formation of the secondary PEC aggregates and their final size, stability, and polydispersity are controlled by Coulomb interactions between charged primary PEC nanoparticles. Computer simulation techniques can be particularly useful for study of such processes.

This chapter is organized as follows: Section 2 reviews the main equations describing important interactions between dissimilar colloidal particles. The contributions of Born repulsion, van der Waals, electrostatic, structural solvation, and hydrophobic hydrodynamic interactions, as well as the effects of attraction between like-charge colloids, charge nonuniformity, and adsorbed polymer are analyzed. Section 3 presents the main types of computer models used for simulation of cluster morphology and results for different interacting species (similarly and oppositely charged particles and polyelectrolytes) and different models (DLA-like, Eden-like). Section 4 considers the classical Smoluchowski model, the theoretical approach of population balance equations (PBE), classification of kernels, and the main types of scaling in aggregation behavior. The recent data on aggregations kinetics of charged PEC particles are also presented.

## 2 Interactions Between Colloidal Particles

The Derjaguin–Landau–Verwey–Overbeek (DLVO) theory is commonly used to describe interactions of charged surfaces across liquids [8, 9]. The DLVO theory models the interparticle interactions by superposing van der Waals attractions and electrostatic double layer repulsion forces. The direct force measurements have confirmed this theory down to surface separations of few nanometers [10].

The important characteristic of electrolytes are the Bjerrum length,  $\lambda_B$ , and Debye length,  $\lambda_D$ , defined as:

$$\lambda_B = \frac{e^2}{4\pi\epsilon\epsilon_0 k_B T}, \quad (1)$$

$$\lambda_D = \sqrt{\frac{\epsilon\epsilon_0 k_B T}{2\rho e^2}}. \quad (2)$$

Here,  $\epsilon$  and  $\epsilon_0$  are the dielectric constants of the medium and vacuum, respectively,  $k_B$  is the Boltzmann constant,  $T$  is the absolute temperature,  $\rho$  is the number density of the added salt,  $e$  is the charge of an electron, and  $\lambda_D = (\sqrt{8\pi\lambda_B\rho})^{-1}$ .

The value of  $\lambda_B$  is defined as the distance at which the interaction between two elementary charges equals  $k_B T$ . At room temperature in water,  $T = 298$  K and  $\lambda_B = 56/\epsilon \approx 0.7$  nm. At this condition, the dissociation energy of the ionic pair with a distance  $R \cong 0.7$  nm between the opposite charges  $u_d = k_B T \lambda_B / R$  is of order

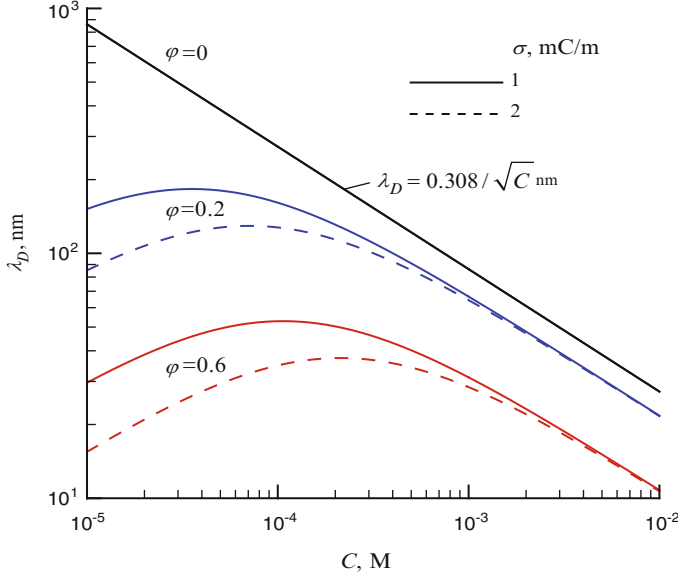


**Fig. 1** Debye screening length,  $\lambda_D$ , versus the molar concentration of salt,  $C$ , at different volume fractions  $\varphi$  and surface charge densities  $\sigma$  of colloidal particles. The radius of particles,  $r$ , was 85 nm

of  $k_B T$  and the ionic pair is unstable. However, such an ionic pair may be stable in less polar solvent.

The Debye length,  $\lambda_D$ , at room temperature may be estimated as  $\lambda_D = 0.308/\sqrt{C}$  nm, where  $C$  is the molar concentration of salt ( $1 \text{ M} = 10^3 \text{ mol m}^{-3}$ ). Note that when the volume fraction of colloidal particles  $\varphi$  is not low, the Debye length  $\lambda_D$  becomes dependent on  $\varphi$ , colloidal particle radius,  $r$ , and colloidal particle surface charge density,  $\sigma$  [11]:

$$\lambda_D(\varphi) = \lambda_D(0) \sqrt{\frac{1 - \varphi}{1 + 1.5\sigma\varphi/(epr)}}. \quad (3)$$

The  $\lambda_D(\varphi)$  dependence becomes important when the volume fraction of particles,  $\varphi$ , is large, or the concentration of salt  $C$  is very low. Moreover, the value of  $\lambda_D$  passes through a maximum with increase in  $C$  (Fig. 1).

## 2.1 van der Waals Interactions

According to the Derjaguin approximation [12], the energy of van der Waals interactions between spherical particles of radii  $r_i$  and  $r_j$  is:

**Table 1** Examples of Hamaker constants for different materials [13]

Medium	Hamaker constant, $A$ ( $\text{J}/10^{-20}$ )
Polystyrene	7.8
Poly(methyl methacrylate)	7.1
Silica	6.5
Quartz	11.0–18.6
Water	3.3–6.4
Pentane	3.8
Ethanol	4.2
Cyclohexane	5.2

$$\begin{aligned}
 u_w(h) &= -\frac{A}{6} \left( \frac{2r_i r_j}{R^2 - (r_i + r_j)^2} + \frac{2r_i r_j}{R^2 - (r_i - r_j)^2} + \ln \left[ \frac{R^2 - (r_i + r_j)^2}{R^2 - (r_i - r_j)^2} \right] \right) \\
 &= -\frac{A}{6} \left( \frac{2}{S^2 + 4Sx} + \frac{2}{S^2 + 4Sx + 4} + \ln \left[ \frac{S^2 + 4Sx}{S^2 + 4Sx + 4} \right] \right), \quad (4)
 \end{aligned}$$

where  $h$  is the surface-to-surface separation distance,  $R = h + r_i + r_j$  is the distance between the centers of particles,  $A$  is the Hamaker constant,  $S = h/\bar{r}_g$ ,  $\bar{r}_g = \sqrt{r_i r_j}$  is the mean geometrical radius, and  $x = \bar{r}/\bar{r}_g$ ,  $\bar{r} = (r_i + r_j)/2$  is the mean radius.

At small separation distance, i.e., at  $h \ll \bar{r}_g$ , the energy of van der Waals interactions is inversely proportional to the surface-to-surface separation distance:

$$u_w(h) \approx -\frac{A}{6} \frac{r^*}{h}, \quad (5)$$

where  $r^* = 2r_i r_j / (r_i + r_j)$ .

The value of  $A$  corresponds to the effective Hamaker constant for the interaction between particles  $i$  and  $j$  in the dispersion medium. The values of the Hamaker constant are presented for different materials in Table 1.

The effective value of  $A_{123}$  is related to Hamaker constants of individual materials  $A_{11}$ ,  $A_{22}$ , and  $A_{33}$  and can be estimated as [14]:

$$A_{123} = \left( \sqrt{A_{11}} - \sqrt{A_{33}} \right) \left( \sqrt{A_{22}} - \sqrt{A_{33}} \right). \quad (6)$$

For similar particles, i.e., at  $A_{11} \approx A_{22}$ , the value of  $A_{33}$  has a positive sign that corresponds to the attractive van der Waals interactions. However, when the value of  $A_{33}$  is intermediate between those of  $A_{11}$  and  $A_{22}$ , it has a negative sign that corresponds to the repulsive van der Waals interactions.

In fact, the Hamaker constant  $A_{131}$  is not constant but depends on the concentration of electrolyte and on retardation [15]:

$$A_{123} = A_0(1 - 2h/\lambda_D) \exp(-2h/\lambda_D) + A_1 F_R(h), \quad (7)$$

where  $A_0$  and  $A_1$  are the zero-frequency and high-frequency contributions, respectively, and  $F_R$  is the retardation function [16]. The zero-frequency contribution represents the net effect of orientation and induction interactions, and the high frequency term arises from London dispersion interactions. Note that the retardation effect can be ignored for a small distance between the particle surfaces ( $<5\text{--}10$  nm).

In recent years, many investigators, in order to overcome difficulties with simulations, have used the simplified forms of attraction potentials, e.g., the Morse potential [17]:

$$u_M(h) = u_M^0 \exp(-h/\lambda)(\exp(-h/\lambda) - 2), \quad (8)$$

where  $\lambda$  is the range parameter and  $u_M^0$  is the potential well depth.

## 2.2 Electrostatic Interactions

The most popular potential that captures the essential behavior of electrostatic interactions between two equal spherical colloids of charge  $Ze$  is the Yukawa potential:

$$u_Y(R) = \pm u_Y^z \exp\left(-\frac{R-r}{\lambda_D}\right) \frac{r}{R}, \quad (9)$$

where the sign is positive for equally charged particles and negative for oppositely charged particles,  $R = h + 2r$  is the distance between the centers of the particles, and:

$$u_Y^0 = \frac{(Ze)^2 r \exp(r/\lambda_D)}{4\pi\epsilon\epsilon_0}. \quad (10)$$

### 2.2.1 DLVO Approximation

The same form of potential follows from Derjaguin, Landau [8], Verwey and Overbeek [9] (DLVO) theory that invokes the Debye–Hückel approximation to linearize the Poisson–Boltzmann equation:

$$\begin{aligned} u_Y(h) &= \pm \frac{(Ze)^2}{4\pi\epsilon\epsilon_0 R} \frac{\exp(-h/\lambda_D)}{(1 + r/\lambda_D)^2} \\ &= \pm \frac{(Ze)^2 g^2}{4\pi\epsilon\epsilon_0 R} \exp(-R/\lambda_D), \end{aligned} \quad (11)$$

where  $g = \exp(r\lambda_D)/(1 + r\lambda_D)$  is the geometric factor that reflects the absence of screening inside the particle exclusion region.

Equation 11 is only valid in the weak Coulomb coupling regime. For highly charged colloidal particles, strong electrostatic coupling between colloidal particles and ions results in additional screening of  $Ze$ . In a general case, the functional dependence of effective charge  $Z^*e$  on real charge  $Ze$  may be rather complex [18] and can be determined by geometry of particles, distribution of charges on their surface, and concentration of ions.

The extension of the Derjaguin approximation for electrostatic interaction energy between two dissimilarly charged spheres of radii  $r_i$  and  $r_j$  was introduced by Hogg, Healy, and Feurstenau (HHF) [19]. Two expressions that are valid under both constant charge,  $\sigma$ , and constant potential,  $\psi$ , conditions were proposed:

$$u_c(h)^\psi = u_c^0 \left\{ -2 \ln \left[ \frac{1 + e^{-h/\lambda_D}}{1 - e^{-h/\lambda_D}} \right] + \frac{(\zeta_i^2 + \zeta_j^2)}{\zeta_i \zeta_j} \ln(1 - e^{-2h/\lambda_D}) \right\} \quad (12)$$

$$u_c(h)^\psi = u_c^0 \left\{ +2 \ln \left[ \frac{1 + e^{-h/\lambda_D}}{1 - e^{-h/\lambda_D}} \right] + \frac{(\zeta_i^2 + \zeta_j^2)}{\zeta_i \zeta_j} \ln(1 - e^{-2h/\lambda_D}) \right\}, \quad (13)$$

where  $u_c^0 = \pi\epsilon\epsilon_0 r^* \zeta_i \zeta_j$ ,  $r^* = 2r_i r_j / (r_i + r_j)$ ,  $\zeta$  is the zeta-potential, and  $h$  is the surface-to-surface separation distance.

Approximations for electrostatic repulsion in Eqs. 12, 13 are valid for  $h \ll r^*$ , relatively small values of  $\zeta$ ,  $\zeta/z < kT_B/e \cong 25$  mV, and  $r^*/\lambda_D > 10$ . Corrections to the fourth and sixth powers of surface potentials in the HHF formulas have been made in [20]. Other more general formulas can be found in the literature [21].

### 2.2.2 Attraction Between Like-Charge Colloids

Many experimental works have shown that unusual long-range attractive interactions, which cannot be explained by the DLVO theory [22–25], may exist for similarly and highly charged colloidal particles. It is interesting that these interactions were observed only in the presence of charged walls.

The theoretical explanations of this effect are rather controversial [26–28]. A highly charged colloidal particle of charge  $Ze$  captures  $N$  oppositely charged counterions of charge  $ze$ , which form a very thin shell around the charged colloidal particle surface, resulting in a very strong screening. Under certain conditions, the counterions may totally neutralize or even overcharge the colloidal particle [29]. The charge neutrality is fulfilled when the colloidal particle captures  $N = N_n = Z/z$  counterions. In the ground state (i.e. at  $T = 0$ ), the spherical colloidal particle can capture even more positionally correlated counterions and the effective charge of

colloidal particle  $Z^*e$  gains the same sign as that of counterions [26, 30]. Estimations have shown that at  $Z \gg z$  [30]:

$$N \approx N_n + 0.8265\sqrt{Z/z}, \quad (14)$$

and the maximally possible value of  $Z^*$  is:

$$Z^* = (N - N_n)z \propto \sqrt{Zz}. \quad (15)$$

The estimation based on Debye, Huckel, and Bjerrum theory predicts that in the strong Coulomb coupling regime the counterion correlations can give rise to attractions at short separations between particles [31, 32]. The analytical calculations predict that the effective long-range interactions between like-charge colloids immersed in a confined electrolyte are repulsive [33]. However, the possibility of long-range attractions arising from charge fluctuations was theoretically predicted [34]. Recent extensive theoretical and computer simulations have shown the important role of counterion correlations [32, 35] and charge fluctuations of either colloidal particles [36], or condensed counterions [37].

The experimentally observed attractive interactions between like-charged colloidal spheres [25] were explained by a nonequilibrium hydrodynamic effect [38]. A mechanism was also proposed based on formation of the depletion zone of counterions between nearly touching like-charged colloidal particles [39].

According to Manning's theory [40], the rodlike polyelectrolyte can capture  $N$  oppositely charged counterions:

$$N = (1 - 1z\zeta)Z/z, \quad (16)$$

where  $\zeta = \lambda_B/b$  is the coupling strength.

The theory predicts that attraction is possible only in the presence of multivalent counterions and if the number of counterions condensed on polyions exceeds [41]:

$$N > N_n/2 = Z/2z \gg 1. \quad (17)$$

So, attraction is possible only for polyelectrolytes with a high coupling strength,  $\zeta > 2/z$ .

Taking into account the many-body interactions between highly charged colloids and counterions, Tokuyama proposed the following equation for effective attractive potential [42, 43]:

$$u_T(R) = u_T^0 \left\{ (Z/z)^3 F(\lambda_m/R) - F(\lambda/R) \right\}, \quad (18)$$

where  $u_T^0 = 0.5k_B T (Zz\lambda_B/\lambda_D)^2$ ,  $R = h + 2r$  is the distance between the centers of particles,  $Ze$  and  $ze$  correspond to the bare charges of colloid particles and counterions, respectively,  $\lambda_m = \lambda_B \sqrt{z/Z}$ , and  $F(x) = (x - 1)x \exp(-x) - \int_x^\infty y^{-1} \exp(-y) dy$ .



Note that this type of potential was used in Brownian-dynamics simulations of charged colloidal suspensions, where gas, liquid-droplet, and crystal-droplet phases were identified [44].

### 2.2.3 Effect of Charge Nonuniformity

The charge nonuniformity on the surface of colloidal particles may also significantly contribute to the electrostatic interactions. It can arise from selective ion adsorption on the surface of colloidal particles and distribution of  $\zeta$  potential [45, 46]. The surface charge nonuniformity can lead to attractive electrostatic and hydrophobic interactions between particles and cause suspension instability [47–49]. An extension of the HHF model for the randomly charged surfaces gives the following Velegol–Thwar potential [46]:

$$u_v(h)^\psi = u_e^0 \left\{ 2 \ln \left[ \frac{1 + e^{-h/\lambda_D}}{1 - e^{-h/\lambda_D}} \right] + \frac{(\zeta_i^2 + \zeta_j^2 + \sigma_i^2 + \sigma_j^2)}{\zeta_i \zeta_j} \ln(1 - e^{-2h/\lambda_D}) \right\}, \quad (19)$$

where  $u_e^0 = \pi \epsilon \epsilon_0 r^* \zeta_i \zeta_j$ , and  $\sigma$  is the variance of the surface  $\zeta$  potential.

### 2.3 Born Repulsion

Short-ranged repulsion between the cores of colloidal particles (assuming that the particles cannot interpenetrate) may be approximated by the Born potential [50]:

$$u_B(h) = -\frac{u_B^0}{R^*} \left( \frac{R^{*2} - 14R^* + 54}{(R^* - 2)^7} + \frac{-2R^{*2} + 60}{R^{*7}} + \frac{R^{*2} + 14R^* + 54}{(R^* + 2)^7} \right), \quad (20)$$

where  $R^* = R/2r$ ,  $R$  is the distance between the centers of the particles, and value of  $u_B^0$  determines the primary minimum of potential.

### 2.4 Structural Solvation Interactions

Direct measurement using atomic force microscopy has shown the presence of short-range repulsion or attraction solvation forces between colloidal particles. These forces reflect the finite size of the solvent molecules and are important only at certain values of pH and electrolyte concentrations. The distance

dependence of the structural solvation potential may be approximated as was first described by Marcelja and Radic [13, 51]:

$$u_s(h) = u_s^0 \exp(-h/\lambda_s), \quad (21)$$

where  $u_s^0 = rp_s\lambda_s^2$ ,  $p_s$  is the structural pressure constant, and  $\lambda_s$  (approximately 0.2–2 nm) is the solvation decay length. Usually, the monotonic exponential decay superimposes on an oscillatory profile.

## 2.5 Hydrophobic Interactions

Hydrophobic interactions are rather typical for organic colloidal particles (e.g., the particles of latex) dissolved in water. They produce a net attractive contribution. The hydrophobic potential for two equal spherical colloidal particles is expressed as [13]:

$$u_h(h) = -u_h^0 \exp(-h/\lambda_h), \quad (22)$$

where  $u_h^0 = 2\pi r\gamma\lambda_h$ ,  $\gamma$  ( $\sim 10 - 50 \text{ mJ/m}^2$ ) and  $\lambda_h$  ( $\sim 1 - 2 \text{ nm}$ ) are empirical parameters.

This contribution is rather short-ranged and reduces only the height of the DLVO potential barrier without modifying the depth of the secondary minimum [52].

## 2.6 Effect of Polymers

### 2.6.1 Adsorbing Polymer

Polymer adsorption may result in bridging attraction or steric repulsion between two particles. The scaling theory of polymer adsorption that accounts for the interaction between the polymer and the surface and for variation of polymer concentration near the surface [53, 54] was used for derivation of the interaction potential between two spherical colloidal particles coated by polymer [55–57]:

$$u_p^a(h) = u_p^0 \left[ -\ln(2\delta/h) + \sqrt{2}\Gamma^{5/4} \left( (\lambda_p/h)^{1/4} - (\lambda_p/2\delta) \right)^{1/4} \right], \quad (23)$$

where  $u_p^0 r v k_B T / (a_m^3) 16 \varphi_p^{9/4} \lambda_p^2 \Gamma$ ,  $v$  is the numerical constant,  $a_m$  is the effective monomer size,  $\varphi_p$  is the polymer volume fraction at a single surface,  $\Gamma$  is the degree of surface saturation by the adsorbed polymer (fractional polymer surface coverage),  $\delta$  is the thickness of the adsorbed polymer layer, and  $\lambda_p$  is the scaling length, which is a measure of the segment surface interactions.

The first term within the square brackets in Eq. 23 corresponds to the short-range bridging attraction and the second term is for steric (excluded volume) repulsion.

### 2.6.2 Non-adsorbing Polymer

Depletion of attraction caused by the presence of a non-adsorbing polymer may be calculated as [10]:

$$u_p^n(h) = -u_p^0(1 - 3t/4 + t^3/16), \quad (24)$$

where  $u_p^0 = 4\pi p_0(r + \delta)^3/3$ ,  $p_0$  is the osmotic pressure in the bulk,  $\delta$  is the exclusion thickness, and  $t = (2r + h)/(a + \delta)$ .

## 2.7 Hydrodynamic Interactions

Hydrodynamic interaction mediated by the solvent originates from the movement of particles and occurs when particles are close to each other. It is determined by the viscous drag dependence on interparticle distance [16, 58] and results in a decrease in the particle diffusion coefficient by the factor  $\beta$ , i.e.,  $D = D_0\beta$  [59, 60]. Here,  $D_0$  is the diffusion coefficient of a particle in the infinitely diluted solution. For motion along the line of the particle centers, the exact expression for  $\beta$  was obtained by Brenner [61] and was approximated by the following rational function [62]:

$$\beta(h/r) \simeq \frac{6(h/r)^2 + 13(h/r) + 1}{6(h/r)^2 + 4(h/r)}. \quad (25)$$

Formally, hydrodynamic repulsion energy  $u_{hd}$  may be expressed as the following correction to the total energy:

$$u_{hd}(h) = k_B T \ln \beta(h/r). \quad (26)$$

The effect of hydrodynamic interactions on aggregation of colloidal particles may be rather essential and simulation results show that they constrain the growth of aggregates [63]. Computational simulation predicts that many-body hydrodynamic interactions between colloidal particle are able to reduce the solid fraction required for percolation or gelation [64, 65]. The merging of clusters into condensed aggregate was observed at particle volume fraction  $\varphi$  as low as 0.06–0.12 [64].

In concentrated suspensions of charged colloidal particles, the strong Coulomb interaction prevents the particles from moving freely and leads to an effective screening of hydrodynamic interaction [66]. Such a screening may be particularly

important in polyelectrolyte solutions with strong coupling of electrostatic and hydrodynamic interactions between the polymer chains [67, 68].

## 2.8 Interaction Between Colloidal Aggregates

Until recently, there was no clear conception about interaction between two aggregates consisting of many individual particles. Practically all efforts were devoted to studies of interactions between single particles with an idealized shape, e.g., spheres, cylinders, and ellipsoids.

The general schema of calculation of the van der Waals interaction energy between irregularly shaped molecular aggregates was developed in 1998 [69]. More recently, the calculations of van der Waals and double layer interactions between colloidal aggregates were performed [70, 71]. The direct numerical calculations of the van der Waals interaction between fractal aggregates of colloidal particles (based on a pairwise summation of interaction energies between all particles) have shown that they can be fairly well approximated by the energy of interaction between the closest pair of primary particles [70]. However, it was noted that the surface distance between two aggregates is governed by the morphology of clusters and there may be an apparent impact on the van der Waals interaction. Similar estimations were done for the double layer interactions between fractal or hexagonal closed-packed aggregates with considerable overlapping of double layer inside the aggregates and between two interacting aggregates [71]. It was shown that for the relatively thin double layer ( $\lambda_D \leq 0.2r$  for closed-packed aggregates and  $\lambda_D \leq r$  for aggregates with a small fractal dimension), the interaction of aggregates is close to the interaction of the nearest pair of the primary particles. However, in thick double layers ( $\lambda_D > r$ ), the overlapping of the double layer inside the aggregate was noticeable and formation of a spheroidal double layer around the aggregate was observed.

## 3 Simulation of Cluster Morphology

A number of theoretical models and computer simulation approaches were developed for description of the cluster morphology [72], reaction kinetics, and time dependence of the cluster-size distributions [73].

### 3.1 Main Types of Computer Models

The cluster morphology may depend on details of colloidal particle interactions, mechanism of particle attachment to the cluster, and dimensionality of the problem. The existing models for cluster morphology simulation account for the trajectory of

the moving particles (diffusion limited aggregation, DLA; reaction limited aggregation, RLA; ballistic aggregation, BA; and Eden-like aggregation) [74].

In the DLA model, the individual particles or clusters stochastically diffuse via Brownian trajectories towards one another and every collision between them results in formation of a larger cluster [75]. The clusters formed display a fractal morphology that depends upon the space dimension in the DLA model. In the RLA model, the probability of attachment is small and only a small fraction of collisions between clusters leads to formation of larger clusters. Traditionally, DLA and RLA are called rapid and slow aggregations, respectively.

A similar mechanism of aggregation is used in the BA model; however, here the trajectories of moving particles are assumed to be linear [76–78]. In the Eden-like aggregation model, new single particles attach to the cluster at its perimeter [79]. The type of diffusion motion strongly affects the cluster morphology, e.g., Brownian motion generates typical fractal DLA clusters, linear trajectories lead to compact structures, and Levy-flight trajectories allow continuous changes of the cluster morphology [80].

The above models are irreversible. Finally, it is expected that clusters grow and merge until formation of a single connected cluster. However, the experimental studies show that some systems can display the presence of reversible aggregation. In a rapid aggregation process, the clusters with loose structure arise initially, and after a certain time they can restructure to more compact clusters with higher fractal dimensionality [81, 82]. The process of thermal restructuring of fractal polymer clusters dispersed in water was experimentally observed using small-angle light scattering [83].

In the absence of aggregation, restructuring resulted in an increase in the fractal dimension. A simple model of the restructuring kinetics, based on coalescence theory of liquid droplets, was developed [83]. Reversible-growth models were also built. These models allow unbinding of particles and imply that later on, during the restructuring, the ramified clusters become compact [84, 85]. The details of cluster morphology strongly depend on the interparticle interaction, the presence of restructuring, and external fields [86]. Impact of interactions on the intrastructure of colloidal clusters was recently studied by Brownian dynamics simulations [17]. It was shown that an increase in density of suspension results in stronger intercluster interactions that affect the intrastructure of clusters. However, perturbation of the intrastructure of clusters was shown to be low in diluted suspension.

### 3.2 *Similarly Charged Particles*

For colloidal suspensions, the influence of the combination of short-range attractions and long-range repulsions on clustering phenomena [87] is extremely interesting. It is expected for charged particles that cluster accumulates net charge and may reject association of additional particles at a certain critical size.

The long-range repulsion may result in limitation of the cluster size [87, 88]. Coulomb repulsion tries to break charged spherical clusters or introduce an ellipsoidal deformation [89, 90]. In 1935, Weizsacker studied the stability of the atomic nucleus by analyzing the potential energy of the charged spherical cluster  $u_t$  [91]. In the case when the cluster is filled by  $N$  primary particles with radius  $r$  and charge  $Ze$ , the value of  $u_t$  includes the volume  $u_v$ , surface  $u_s$ , and electrostatic  $u_e$ , terms:

$$u_t(N) = u_v + u_s + u_e = -u_0N + aN^{2/3} + bN^{5/3}, \quad (27)$$

where  $u_0$  is the binding energy per particle,  $a = 4\pi\gamma r^2\phi^{-2/3}$  is the surface tension parameter,  $b = 3k_B T \lambda_B \phi^{1/3}/5r$  is the electrostatic repulsion parameter,  $\gamma$  is the surface tension at the interface between the aggregate and solvent,  $\phi$  is the volume fraction of particles in the aggregate, and  $\lambda_B = (Ze)^2/(4\pi\epsilon\epsilon_0 k_B T)$  is the Bjerrum length for primary particles in the aggregate.

The radius of a spherical cluster may be calculated as:

$$r^c = r(N/\phi)^{1/3}. \quad (28)$$

Figure 2 shows examples of dimensionless total potential energy of a spherical cluster,  $u_t/u_0$ , versus the number of primary particles,  $N$ , at a fixed value of  $a$  ( $a/u_0 = 2$ ) and different values of  $b/u_0$ . The clusters are definitely stable at  $u_t < 0$ . At relatively small charge  $Z$  of the primary particles, the curve  $u_t$  goes through the maximum (see, inset in Fig. 2) at:

$$N_1^{\max} = \left(\frac{2a}{3u_0}\right)^3 \left(1 + \frac{20a^3b}{9u_0^3}\right), \quad (29)$$

and bigger clusters are stable (i.e.  $u_t < 0$ ) in the certain range of  $N$  values.

A noticeable change in the shape of the  $u_t$  curve is observed for a charged cluster (Fig. 2), e.g., at  $a = 0$ , i.e. in absence of surface tension, the  $u_t$  function curve goes through the minimum and has two zeros at  $N = 0$  and at:

$$N = N_2^{\max} = (1/b)^{3/2} = \left(\frac{5}{3\phi^{1/3}} \frac{r}{\lambda_B} \frac{u_0}{k_B T}\right)^{3/2}. \quad (30)$$

Note that the critical size  $N_2^{\max}$  corresponds to the physical situation when the next primary particle cannot attach to the compact spherical cluster. In principle, the cluster grown may continue through formation of noncompact branching morphology structures with smaller value of  $\phi$ . Thus, the critical size  $N_2^{\max}$  corresponds to development of morphological instability.

Stability analysis with respect to ellipsoidal deformation has shown that even bigger clusters (initially formed and then becoming charged) may lose stability and dissociate on smaller clusters (Fig. 2) at certain critical size:

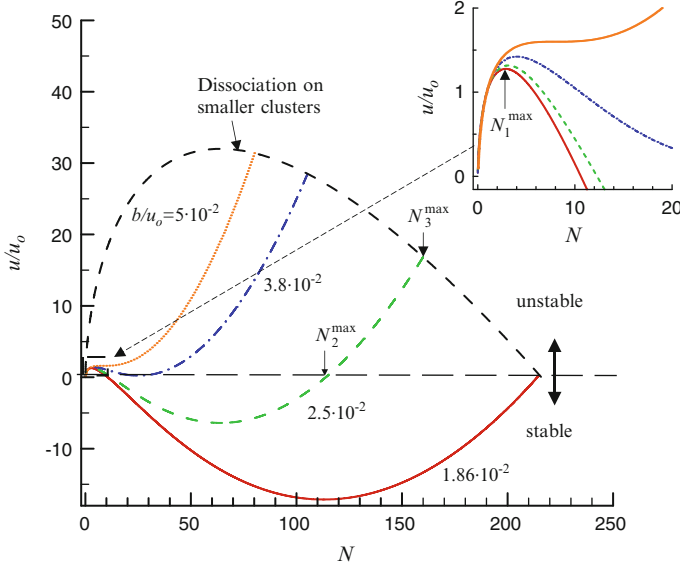


**Fig. 2** Dimensionless total potential energy of a spherical cluster,  $u_t/u_0$ , versus the number of primary particles,  $N$ , at  $a/u_0 = 2$  and at different values of  $b/u_0$ . *Inset* shows the enlarged part of this figure at small values of  $u_t/u_0$  and  $N$

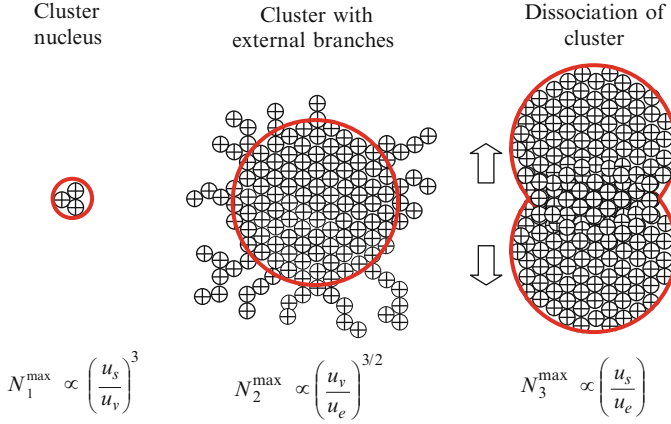
$$N = N_3^{\max} \approx 2a/b = \frac{10}{3\varphi} \frac{r}{\lambda_B} \frac{4\pi\gamma r^2}{k_B T} \quad (31)$$

that corresponds to development of dissociative instability.

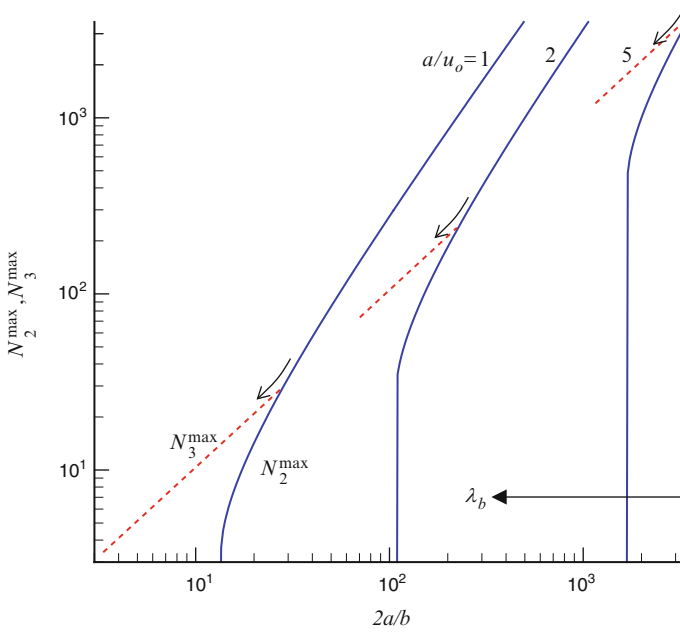
In both Eqs. 30 and 31, the larger cluster corresponds to the larger ratio of  $r/\lambda_B$  and smaller value of  $\varphi$ . The stable growth regime is expected for zero value of  $\lambda_B$  ( $b = 0$ ), which corresponds to formation of an infinite cluster or gel-like phase. However, the completely unstable growth regime is expected when  $\lambda_B$  exceeds some critical value. In this case, the value of  $u_t$  is positive at any value of  $N > 0$  (see, e.g., the case of  $b/u_0 = 3.8 \times 10^{-2}$  in Fig. 2). Energetically, the critical sizes  $N_1^{\max}$ ,  $N_2^{\max}$  and  $N_3^{\max}$  are controlled by ratios  $u_s/u_0$ ,  $u_c/u_c$  and  $u_s/u_0$ , respectively (Fig. 3).

Figure 4 compares  $N_2^{\max}$  and  $N_3^{\max}$  versus ratio  $2a/b$  behavior for fixed values of  $a$  (surface tension parameter). The slightly charged clusters (small values of  $\lambda_D$ ) can grow to larger size and the values of  $N_3^{\max}$  and  $N_2^{\max}$  coincide. In this unstable grown regime, the morphological and dissociative instabilities develop simultaneously. For highly charged clusters (large values of  $\lambda_D$ ), the value of  $N_3^{\max}$  may noticeably exceed the value of  $N_2^{\max}$  at certain critical  $\lambda_D$ .

In principle, these general considerations are consistent with recent experimental and computer simulation results. The finite-size clusters were experimentally realized in suspensions of colloidal particles with interactions induced by a non-adsorbing polymer [92, 93]. Cluster morphology was dependent on the range of the



**Fig. 3** The critical sizes of charged cluster  $N_1^{\max}$ ,  $N_2^{\max}$  and  $N_3^{\max}$ . The values of  $N_1^{\max}$ ,  $N_2^{\max}$  and  $N_3^{\max}$ , correspond to the formation of initial nucleus, growth of external branches, and dissociation of charged droplets, respectively



**Fig. 4** Maximum cluster sizes  $N_2^{\max}$  and  $N_3^{\max}$  versus ratio  $2a/b$  at fixed values of  $a/u_0 = 1, 2$ , and  $5$

interaction and was becoming more compact for longer range interactions. The origin of such behavior is not completely clear so far.

The large charged clusters may be unstable with respect to formation of elongated or linear structures. The theory predicts formation of near-linear chains with



small fractal dimension,  $d_f \sim 1$ , in polyelectrolytes in the limit of high electrostatic interactions ( $\lambda_B \sim 0.1$  nm) [94]. Formation of linear structures was observed also in Monte Carlo simulations of a short polyelectrolyte with various numbers of beads,  $N = 8\text{--}80$  [95]. The value of  $d_f$  was noticeably increasing as Bjerrum length  $\lambda_B$  decreased.

The effect of the range of interactions on the structural and kinetic properties of a computer-simulated two-dimensional aggregating colloidal system was studied using the repulsive Yukawa potential [96] (Eq. 9). The increase in  $\lambda_D$  or  $u_0$  provokes arrangement of aggregates into linear structures. The repulsive interactions also have a strong influence on the kinetic behavior of the coagulation process. The structure of small clusters composed of up to 80 particles interacting simultaneously via attractive and repulsive forces was recently simulated [97]. A short-range attraction was simulated by generalization of the Lennard–Jones potential and a long-range repulsion was simulated by the screened electrostatic Yukawa potential. The competition between attraction and repulsion resulted in formation of stable clusters, and the ground-state clusters were preferentially growing almost in one dimension. The extensive numerical simulations were done for suspended charged colloidal particles at a screening length comparable to the particle radius [98]. It was shown that at low temperature, particles organize into quasi one-dimensional aggregates connecting via branching mechanism into a percolating gel structure. Note that experimental data indicate a more elongated and open morphology of the fractal-like aerosol agglomerates at larger charge [99].

### 3.2.1 DLA-Like Model

The impact of long-range interactions on cluster morphology has been intensively studied for different variants of the DLA model [100–103]. It was shown using a quasi-deterministic two-dimensional (2D) particle–cluster growth model with attractive cluster–particle forces proportional to  $R^{-\alpha}$  that the growing cluster was dendritic. Moreover, strong reduction of the fractal dimension,  $d_f$ , with increase in  $\alpha$  was observed [100]. The 2D DLA model with the power-like potential,  $u(R) = u_0 R^{-\alpha}$ , was also studied [101, 104]. Here,  $u_0$  and  $\alpha$  are parameters. Note that this model is equivalent to the ordinary DLA in the limits of short range interactions,  $\alpha \rightarrow \infty$ , or  $u_0 = 0$ . In this problem, the aggregates were grown on a triangular lattice and the effects of anisotropy were important.

The detailed structure of clusters was strongly dependent on  $\alpha$ , or  $u_0$ , e.g., in the case of attractive interactions at large  $|u_0|$  and long-range interaction (i.e., for small  $\alpha$ ), the clusters grew with stable tips and were of dendritic shape. The observed effects reflected the anisotropy induced by the underlying lattice that stabilized the tips of the growing arms. In the limit of small  $|u_0|$  and large  $\alpha$ , the transition from dendritic to tip-split aggregates was observed. At fixed value of  $u_0$ , the estimated fractal dimension  $d_f$  increased with increase in  $\alpha$ , which reflected tip destabilization [101].

The similar cluster–cluster variants of DLA aggregation with either attractive or repulsive interactions were also studied [102, 103]. These simulations were done

using off-lattice models both for 2D [103] and three dimensional (3D) [102] systems. The interaction energy  $u_{ij}$  of two non-overlapping clusters including  $i$  and  $j$  particles was approximated by the power law:

$$u_{ij} = u_0 \sum_{k=1}^i \sum_{l=1}^j R_{kl}^{-\alpha}, \quad (32)$$

where  $R_{kl}$  is the distance between the  $k$ th particle in the cluster  $i$  and  $l$ th particle in the cluster  $j$ .

Both the theory and simulation results gave the following estimates for fractal dimensionality  $d_f$  versus parameter  $\alpha$  dependence:

$$d_f = \begin{cases} d_0, & \alpha > 2d_0 \\ d_0(\alpha + 2)/(2(d_0 + 1)), & 1 < \alpha \leq 2d_0, \end{cases} \quad (33)$$

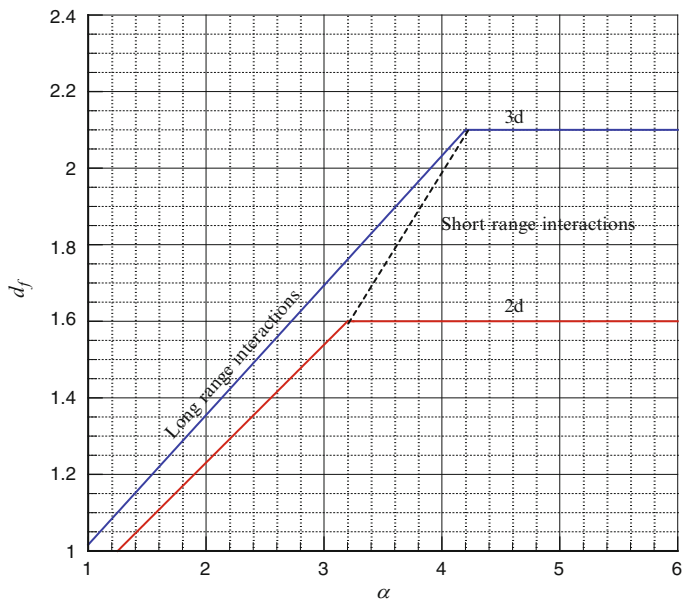
where  $d_0$  is the fractal dimensionality in the cluster–cluster aggregation model without interactions. It equals  $d_0 \sim 1.6$  and  $d_0 \sim 2.1$  for 2D and 3D systems, respectively.

Figure 5 presents  $d_f$  versus  $\alpha$  dependencies for 2D and 3D systems. The figure shows that short range interactions ( $\alpha > 2d_0$ ) do not change the value of  $d_f$ , but long range ( $1 < \alpha \leq 2d_0$ ) interactions lead to substantial changes in  $d_f$ . Moreover, long range interactions can have an important effect on the local structure of clusters [102, 103]. The shape and size of the aggregates may be sensitively dependent on the balance between attraction and repulsion interactions [98].

### 3.2.2 Eden-Like Model

The stochastic Eden-like model of aggregation of the charged particles in 2D systems was developed [105, 106]. In this model, the particles overcome the electrostatic repulsive barrier created by the aggregate and stick to it due to the existence of short-range attractions.

By variation of two model parameters, the screening length,  $\lambda$ , and the attractive binding energy per particle,  $u_0$ , formation of the aggregates with the following morphologies was studied: linear or near-linear, linear with bending, worm-like, dense-branching or dense-branching with a core, and compact Eden-like aggregates. Figure 6 presents an example of a cluster with a charged core and external branches. The regions of finite and infinite growth of clusters with different morphologies are presented in the form of a diagram as  $\lambda$  versus  $u_0$ . The structure and fractal properties of the ramified clusters were studied. It was found that the clusters did not reveal the fractal properties at any values of  $\lambda$  and  $u_0$  and a sharp transition between linear ( $d_f = 1$ ) and dense-branching ( $d_f = 2$ ) morphologies was observed.



**Fig. 5** Fractal dimensionality  $d_f$  versus power exponent  $\alpha$  for 2D and 3D cluster–cluster DLA model

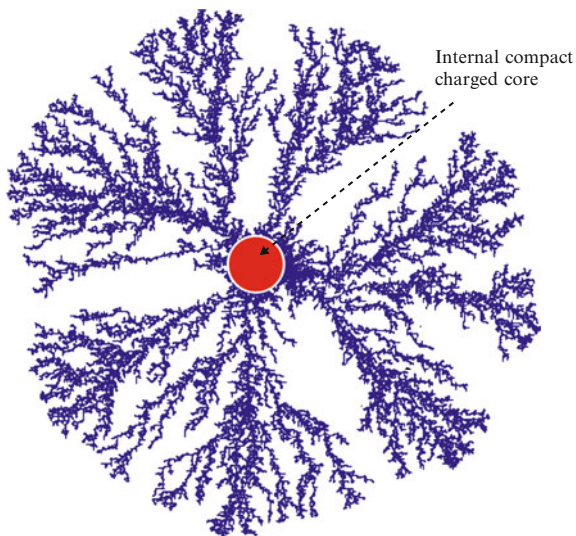


**Fig. 6** Internal structure of cluster obtained using Eden-like model of aggregation of charged particles ( $\lambda = 1$ ,  $u_0 = 60$ ). The cluster includes a core (central dense charged part) and external branches [105]

### 3.3 *Oppositely Charged Particles*

#### 3.3.1 Simple Colloids

The particles of a mixture of oppositely charged nanoparticles form charged aggregates (complexes), in which each charged particle is screened by a shell of oppositely charged particles [107, 108]. The stable core-and-shell aggregates were confirmed in experiments with the mixtures of oppositely charged metal nanoparticles [107]. When the net charges of positive and negative species are equal, the aggregates are neutral and condense into a macroscopic drop, i.e., the system becomes unstable. The theory developed in [109] predicts a possibility of enhanced aggregation of larger charged particles induced by the small polyions of the opposite charge. This phenomenon may reflect the partial “condensation” of the small particles and reduction of the strong electrostatic repulsion between screened (larger) colloidal particles.

The Brownian dynamic simulation of aggregation between the oppositely charged particles has shown that heteroaggregation produces more branched aggregates than the usual diffusive aggregation [110]. Moreover, the cluster discrimination was observed at the late stages of aggregation, when neutral clusters were disappearing faster than charged ones [111].

The presence of linear chaining with particle charge alternating down a chain in aggregates of the oppositely charged polystyrene spheres was revealed by different experimental techniques and was supported by Brownian dynamics simulation [112]. It was shown that branching of an aggregate composed of oppositely charged particles may be varied from a linear chain structure ( $d_f \sim 1.2$ ) to a structure of diffusion-limited aggregates ( $d_f \sim 1.7$ ) by an increase in concentration of the background electrolyte. Formation of linear chains was explained by the short-range attraction between the oppositely charged particles and long-range repulsion between the identical particles. The experiments and the Brownian dynamics simulations of heteroaggregation between the oppositely charged particles [113–115] has shown that small silica (diameter  $\sim 25$  nm, negatively charged) particles covered the surface of large alumina (diameter  $\sim 400$  nm, positively charged) particles. For small amounts of silica particles, agglomeration of the silica-covered alumina particles was observed, and it was demonstrated that the agglomerates were of elongated shape.

#### 3.3.2 Polymers

Behavior of solutions of oppositely charged polymers is rather similar to that of solutions of oppositely charged colloids. However, higher flexibility of the polymer chains results in a less ordered structure of the polyion solutions. Pairing of the oppositely charged polyions, their aggregation, and complexation of anionic and

cationic polyelectrolytes have been intensively studied in many theoretical [116–121] and experimental [122–124] works.

The phase diagram of asymmetric positively and negatively charged chains in an oppositely charged polyelectrolyte was theoretically obtained [125]. It was shown that cylindrical and lamellar cluster structures with nonzero net charge were formed at high polymer concentration. Nonuniform distribution of charge along the annealed polyelectrolyte chains was observed [116, 121]. The theoretical predictions and Monte Carlo simulations show that charges accumulate at the ends of chains. [116]. The cluster size distribution functions of the oppositely charged macroions in solution were studied using the Monte Carlo simulations [120]. It was demonstrated that increasing electrostatic coupling results in formation of larger clusters, and a single cluster comprising all the macroions forms at the strongest coupling. The structure of symmetric polycation–polyanion mixtures without salt in good solvents was studied using the Langevin sampling simulation technique and field-theoretic simulation methods [119, 126]. The obtained results allowed explanation of the phenomenon of complex coacervation, a type of phase separation in which dense liquid precipitates coexist with supernatant solvent.

Brownian dynamics computer simulations have shown that variation in electrostatic interactions changed the size, shape, and local density distribution of the complexes formed by terminally charged hyperbranched polymers and oppositely charged neutralizing linear polyelectrolytes [127]. The ultrasoft core model of interpenetrating polycations and polyanions was proposed for investigation of the polyelectrolyte aggregation using different theoretical approaches and molecular dynamic simulations [117]. The clustering and segregation of the oppositely charged species was observed. At sufficiently low temperatures and densities, the oppositely charged polyions tend to form weakly interacting neutral pairs. The break-up of ion pairs was observed with increase in temperature. This was followed by the percolation transition from low temperature dielectric (insulator) state to high temperature ionic (conductor) state [117].

The Monte Carlo simulations were applied to study the complexation, phase separation, and redissolution of polyelectrolyte–macroion solutions [128]. It was shown that introduction of the oppositely charged polyelectrolytes into a stable macroion solution with repelling macroions resulted in a decrease in the solution stability. The system was unstable at macromolecular charge equivalence when a large and loose cluster of macroions and polyelectrolytes was forming. Finally, redissolution of macroions occurred in the excess of polyelectrolyte.

The complexation between a polyampholyte and a charged particle was studied using Monte Carlo simulations [129, 130]. The increasing charge density and particle size resulted in change of configuration of the polyampholyte chain adsorbed on the particle surface. At large charge density and particle size, collapse of the polyampholyte chain on the particle surface was observed [129]. The effects of different model parameters (polyampholyte contour length, nanoparticle surface charge, pH of solvent, ionic concentration, etc.) on possible polyampholyte conformations at the nanoparticle surface were investigated [130].

The process of aggregation of the oppositely charged polyions (positively charged liposomes and negatively charged polyelectrolyte sodium polyacrylate) was studied by means of Monte Carlo simulation [131]. The model accounted for heterogeneous charge distribution at the particle surface, related with the correlated polyion adsorption [46]. Formation of long-living clusters of polyelectrolyte-decorated particles was demonstrated. Molecular dynamics simulations were performed to study the polyampholyte–polyelectrolyte complexes in solutions [124, 132]. It was demonstrated that polyampholyte chain binds to a polyelectrolyte in a way optimizing electrostatic interactions between the ionic groups in both polymeric chains. Formation of the micellar complex by anionic polyelectrolyte and cationic surfactants (in monomeric and dimeric forms) was investigated by molecular dynamics simulation [133]. Results have shown that the dimeric form interacts more strongly with the polyanion and the size of the micellar complex becomes larger with an increase in the surfactant concentration.

### 3.4 *Effect of Dipolar Interactions*

The effects of dipolar interactions on DLA processes were studied in details for 2D and 3D off-lattice models [134–137]. The fractal dimensionality  $d_f$  was a monotonically increasing function of the temperature (or decreasing function of dipolar forces). For example, it varied continuously from about 1.78 for small dipolar interactions to about 1.35 for large dipolar interactions (3D model) [134, 135]. Therefore, the structure of clusters formed at low temperatures or strong dipolar forces was less branched and more open ( $d_f \sim 1$ ) than in free DLA with no interactions. On increase in temperature or decrease in dipolar forces, the value of  $d_f$  reached the limit value of free DLA [136, 137]. The values  $d_f = 1.13 \pm 0.01$  and  $d_f = 1.37 \pm 0.03$  were obtained in the limit of zero temperature for 2D and 3D systems, respectively. Transitions between an ordered, or quasi-ordered, and a disordered phase were also observed for high values of the reduced temperature [138]. The long range correlations between the dipoles were revealed in the low-temperature ordered phase.

## 4 Kinetics of Aggregation

Kinetics of aggregation, coalescence, and annihilation or fragmentation are important in many physical, chemical and biological processes [21, 80, 139–141]. The popular mean field Smoluchowski approach [73] gives good description of simple aggregation systems. However, in the presence of restructuring, long range interactions, and formation of clusters with fractal geometry, more complicated approaches based on computer simulation methods are useful.

### 4.1 Aggregation as a Second-Order Reaction

In the simplest case, only primary particles are present at initial time,  $t = 0$ , with initial number density of  $\rho_0$  and volume fraction of  $\varphi = 4\pi r^2 \rho_0 / 3$ . It can be supposed that in very diluted systems ( $\leq 1\%$  vol) only two particle collisions are important. The regime of “fast” aggregation is assumed, i.e., two primary particles form an aggregate when they “touch” at the distance of  $2r$  between their centers. The disappearance of primary particles can be considered as a second-order reaction [73]:

$$\frac{dn_1}{dt} = -k^f n_1^2, \quad (34)$$

where  $n_1$  is the dimensionless concentration of the primary particles, i.e.  $n_1 = \rho_1 / \rho_0$ , and  $k^f$  ( $s^{-1}$ ) is the fast aggregation rate constant. Note that  $k^f = 1/\tau_a$ , where  $\tau_a$  is the half-aggregation time corresponding to  $n_1 = 1/2$ .

The integration of Eq. 34 gives:

$$n_1 = (1 + t/\tau_a)^{-1}. \quad (35)$$

Estimations show [73]:

$$k^f = 8\pi Dr = \frac{4k_B T \rho_0}{3\eta}, \quad (36)$$

where  $D = \frac{k_B T}{6\pi r \eta}$  is the diffusion coefficient, and  $\eta$  is the viscosity of solvent.

The half-aggregation time of colloidal dispersion,  $\tau_a$ , may be estimated as:

$$\tau_a = 1/k^f = \tau_B / \varphi = \frac{3\eta}{4k_B T \rho_0}, \quad (37)$$

where  $\tau_B = r^2/(6D)$  is the Brownian time. During the Brownian time, the length of diffusion is equal to the radius of the primary particle,  $r$ .

For example, the Brownian time,  $\tau_B$ , of 10 nm particles ( $\eta \sim 0.001$  Pa s) in water at room temperature ( $T = 298$  K) is equal to  $0.76 \times 10^{-6}$  s. Figure 7 presents plots of  $\tau_a$  versus  $r$  at different values of the volume fraction of particles,  $\varphi$ .

In the presence of repulsive interactions, the sticking probability becomes smaller than 1 and the so-called “slow” aggregation regime may be realized. The slow aggregation rate constant,  $k^s$  may be estimated as:

$$k_{ij}^s = k^f w_{ij}, \quad (38)$$

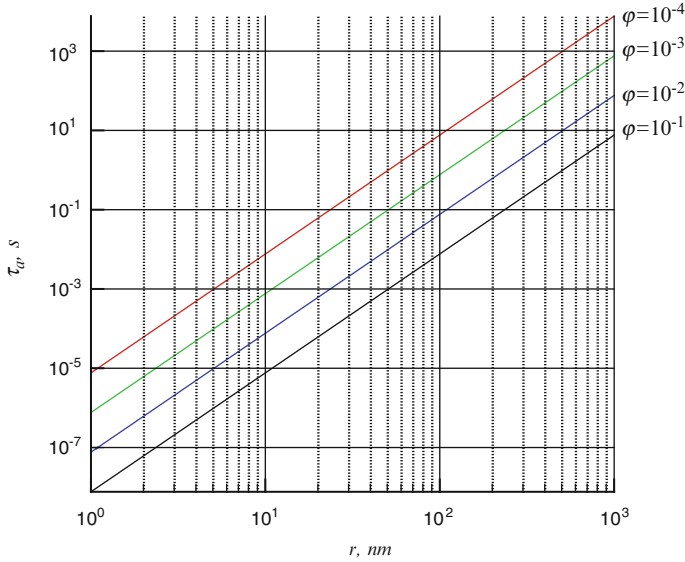


**Fig. 7** Half-aggregation time  $\tau_a$ , versus radius of particle  $r$  at different values of the volume fraction of particles,  $\varphi$ . The estimation was done using Eq. 37 for suspension of particles in water,  $T = 298$  K and  $\eta \sim 0.001$  Pa s

where  $W_{ij} (\geq 1)$  is the dimensionless Fuchs stability ratio, which can be considered as the inverse sticking probability [142]:

$$w_{ij} = \int_0^\infty \frac{\exp(u_t(x)/k_B T)}{(x+2)^2} dx. \quad (39)$$

Here,  $x = h/\overline{r_{ij}}, \overline{r_{ij}} = (r_i + r_j)/2$ , and  $u_t$  is the total energy, i.e., the sum of the attractive,  $u_a$ , and repulsive,  $u_r$ , parts.

It was shown that the value of  $W_{ij}$  is mainly determined by the height of the energy barrier  $u_t^{\max}$  located at  $h \cong \lambda_D$  and the following approximate relation was obtained for equal sized particles,  $r = r_i = r_j$ , [143]:

$$W_{ij} = \frac{\lambda_D}{2r} \exp(u_t^{\max}/k_B T). \quad (40)$$

Usually, it is assumed that fast and slow aggregations are controlled by attractive and total interactions, respectively, and the equation used for estimation of  $W_{ij}$  is more complicated:

$$W_{ij} = \frac{\int_0^\infty dx \exp(u_t/k_B T)/(x+2)^2}{\int_0^\infty dx \exp(u_a/k_B T)/(x+2)^2}. \quad (41)$$



## 4.2 Population Balance Equations

In order to account for formation of dimers, trimers, and larger aggregates, von Smoluchowski proposed in his pioneering work [73] the following system of population balance equations (PBE):

$$\frac{dn_m}{dt^*} = \frac{1}{2} \sum_{i=1}^{m-1} k_{i,m-i} n_i(t) n_{m-i}(t) - n_m(t) \sum_{i=1}^{\infty} k_{m,i} n_i(t), \quad (42)$$

where  $n_m$  is the dimensionless concentration of the clusters of size  $m$ ,  $k_{i,m-i}$  are dimensionless reaction constants, or kernels, and  $t^* = k^f t = t/\tau_a$  is the normalized time.

At initial moment of time,  $t = 0$ , all clusters are assumed to be monomeric and  $n_1 = 1$ . The first term (“birth” term) in Eq. 42 corresponds to the collision between two clusters ( $i$ -mers and  $m - i$ -mers) and formation of  $m$ -mers. In first summation, each collision is accounted for twice; hence, a factor of  $1/2$  is included. The second summation corresponds to the decrease in concentration of  $m$ -mers through aggregation with other clusters.

In fact, the PBE approximation is a mean field approximation valid for dilute systems. Moreover, this approximation does not account for internal structure and differences in the spatial configuration of clusters. For the known functional dependence of  $k_{m,i}$ , time evolution of the cluster population  $n_m(t)$  can be calculated from Eq. 42.

During the aggregation the total mass of clusters:

$$\sum_{i \geq 1} i n_i(t) = 1, \quad (43)$$

is conserved.

The important characteristics of the cluster distributions are dimensionless total number of clusters  $n$ :

$$n(t) = \sum_{i \geq 1} n_i(t) \quad (44)$$

and mean cluster size (mass),  $s(t)$ :

$$s(t) = \sum_{i \geq 1} i^2 n_i(t). \quad (45)$$

**Table 2** Analytical solutions of PBE for constant, sum, and product kernels

Kernel, $k_{ij}$	Concentration of clusters of size $m$ , $n_m$	Number of clusters, $n$	Size of clusters, $s$
2	$\frac{t^*(m-1)}{(1+t^*)^{(m+1)}}$	$\frac{1}{1+t^*}$	$1 + 2t^{*z}$ , $z = 1$
$i + j$	$\frac{(ma)^{m-1} \exp(-ma-t^*)}{m!}$ , $a = 1 - \exp(-t^*)$	$\exp(-t^*)$	$\exp(\alpha t^*)$ , $\alpha = 2$
$2ij$ , at $t^* \leq 0.5$	$\frac{(2mt^*)^{m-1} \exp(-2mt^*)}{mm!}$	$1 - t^*$	$\left(1 - t^*/t_g^*\right)^{-\beta}$ , $\beta = 1$
$2ij$ , at $t^* > 0.5$	$\frac{(m)^{m-1} \exp(-m)}{2mm!t^*}$	$1/(4t^*)$	$\infty$ , gel

Here,  $t^* = t/\tau_a$  is the dimensionless aggregation time [73, 144–146]

### 4.3 Popular Kernels

The analytical solutions of PBE were obtained for some functional forms of kernels, e.g., for constant  $k_{ij} = 2$ , sum  $k_{ij} = i + j$ , and product  $k_{ij} = i + j$  kernels (Table 2). An exact solution exists also for linear combination of these three kernels:

$$k_{ij} = A + B(i + j) + Cij, \quad (46)$$

where  $A$ ,  $B$ , and  $C$  are the arbitrary constants, as well as for  $q$ -sum kernel:

$$k_{ij} = 4 - q^i - q^j, \quad (47)$$

where  $0 < q < 1$ , and for many other kernels (for a review see, [144]).

Figure 8 shows examples of distribution functions  $f(m) = mn_m/(mn_m)_{\max}$  obtained from analytical solutions presented in Table 2 for constant ( $k_{ij} = 2$ ), sum ( $k_{ij} = i + j$ ), and product ( $k_{ij} = 2ij$ ) kernels at different moments in time. It is interesting that at long times the distribution function for the constant kernel has a bell-like shape, whereas for sum and product kernels they monotonically decay with increasing  $m$ .

The case of constant kernel is similar to the situation that was analyzed in Sect. 4.1. The fast aggregation problem with the constant kernel was exactly solved by Smoluchowski in 1917 [73]. This model is based on the more complicated kernel for 3D Brownian aggregation:

$$k_{ij}^B \simeq \frac{1}{2} \left( i^{-1/3} + j^{-1/3} \right) \left( i^{1/3} + j^{1/3} \right) = 1 + (i/j)^{1/3} + (j/i)^{1/3}. \quad (48)$$

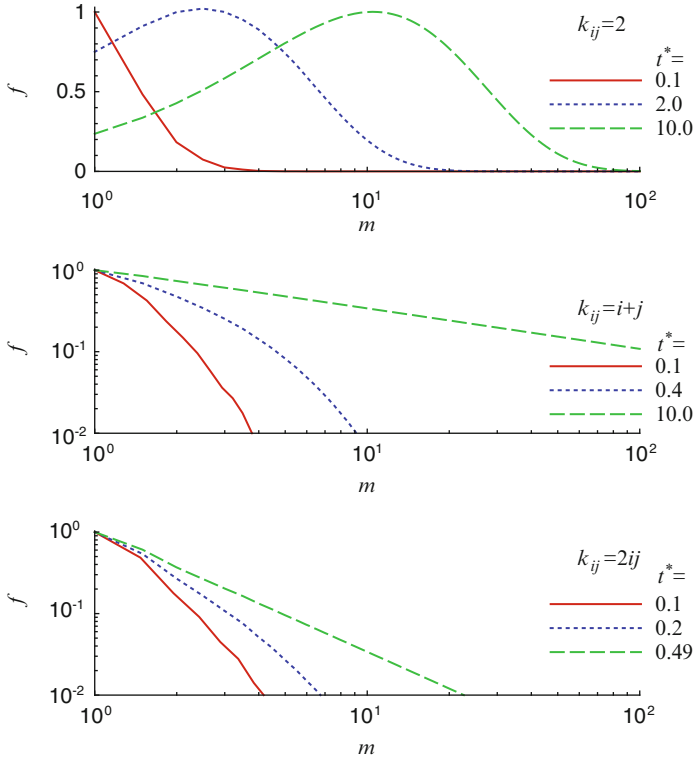


**Fig. 8** Normalized cluster distribution functions  $f(m) = mn_m/(mn_m)_{\max}$  for constant ( $k_{ij} = 2$ ), sum ( $k_{ij} = i + j$ ), and product ( $k_{ij} = 2ij$ ) kernels at different dimensionless times  $t^* = t/\tau_a$

Note that Brownian kernel  $k_{ij}^B$  has a constant value of about 2 when  $i \approx j$ . The kernels for Brownian ( $k_{ijf}^B$ ) or ballistic ( $k_{ijf}^b$ ) aggregation of fractal particles are [147]:

$$k_{ijf}^B \simeq \frac{1}{2} \left( i^{-1/d_f} + j^{-1/d_f} \right) \left( i^{1/d_f} + j^{1/d_f} \right), \quad (49)$$

$$k_{ijf}^b \simeq \frac{1}{2} \left( i^{-1} + j^{-1} \right)^{1/2} \left( i^{1/d_f} + j^{1/d_f} \right), \quad (50)$$

where  $d_f$  is the fractal dimension of the cluster.

The exact analytical solutions of PBE for Brownian and ballistic kernels have not yet been obtained. In slow aggregation regime, these kernel may be estimated as:

$$k_{ij}^{s,B(b)} = k_{ij}^{B(b)} / W_{ij}. \quad (51)$$

Note that the constant kernel kinetics is the slowest as compared to kinetics of the sum and product kernels. It is interesting to note that formation of the infinite

**Table 3** Classification of kernels among three different classes (I, II, III) and gelling (G) or non-gelling (N) behavior

Kernel, $k_{ij}$	Type of kernel	Homogeneity parameter, $\lambda$	Type of cluster union, $\mu$	Class, behavior
2	Constant	0	0	II, N
$i + j$	Sum	$\lambda$	0	II, N
$2ij$	Product	2	1	I, G
$1 + \left(\frac{i}{j}\right)^{1/3} + \left(\frac{j}{i}\right)^{1/3}$	Brownian	$-1/3$	0	III, N
$1 + \left(\frac{i}{j}\right)^{1/d_f} + \left(\frac{j}{i}\right)^{1/d_f}$	Fractal Brownian	$-1/d_f$	0	III, N
$\frac{1}{2} \left(\frac{1}{i} + \frac{1}{j}\right)^{1/2} (i^{1/d_f} + j^{1/d_f})$	Fractal ballistic	$1/d_f - 1/2$	$-1/2$	III, N
—	DLA	0	$\geq 0$	I, N
—	RLA	1	$\geq -1$	I, N

See Fig. 9 for the relationship between  $\lambda$  and  $\mu$  and the behavior and class of kernel, respectively

cluster takes place for the product kernel within the finite time at  $t_g = 0.5\tau_s$ . It corresponds to the sol–gel transition. At time exceeding  $t_g$ , the particles belong to two different populations in the finite (sol phase) and infinite (gel phase) clusters [145].

#### 4.4 Classification of Kernels

For simple aggregation models, the kernel  $k_{ij}$  is usually a homogeneous function:

$$k_{ai,aj} = a^\lambda k_{ij}, \quad (52)$$

where  $a$  is a positive constant and may be presented for large-size clusters as the product of powers  $i^\mu$  and  $j^\nu$  [148]:

$$k_{ij} \simeq i^\mu j^\nu. \quad (53)$$

Here,  $\mu$  and  $\nu$  are exponents,  $\nu = \lambda - \mu$ ,  $i \ll j$ , and  $i \gg 1$ , and kernels with  $\lambda > 2$  and  $\lambda > 1 + \mu$  are unphysical. The values of  $\lambda$  and  $\mu$  for different types of kernels are presented in Table 3.

Figure 9 shows the  $\lambda$  versus  $\mu$  diagram for different types of kernels. The class of the kernel is determined by the sign of the  $\mu$  exponent. The big + big and big + small unions of particles form within the class I ( $\mu > 0$ ) and class III ( $\mu < 0$ ),

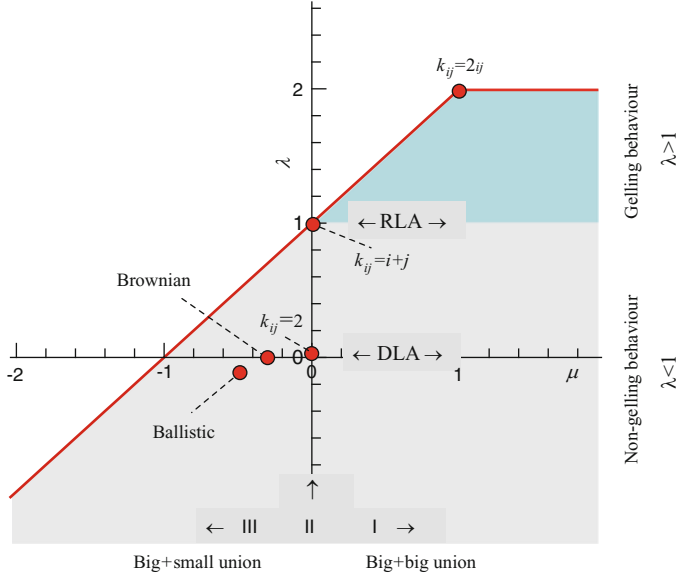


**Fig. 9** Classification of kernels.  $\lambda$  versus  $\mu$  diagram is presented. The shaded area corresponds to the physically plausible limit for  $\lambda (\leq 2)$  and  $\mu (\leq \lambda - 1)$

respectively. For class II ( $\mu = 0$ ), any type of union is probable. The kernels with  $\lambda > 1$  and  $\lambda \leq 1$  correspond to the gelling and non-gelling behavior, respectively. Finally, the well-known regimes of DLA and RSA aggregations correspond to the constant values of  $\lambda = 0$  and  $\lambda = 1$ , respectively. The Brownian aggregation belongs to the DLA-type of aggregation and the sum kernel aggregation belongs to the RLA-type of aggregation. The simple product kernel  $k_{ij} = 2ij$  corresponds to the gelling behavior at the limiting high value of  $\lambda = 2$ .

## 4.5 Dynamic Scaling

It was found in many experimental and theoretical studies of dynamic scaling that the time dependence of cluster distribution for long times, large  $m$ , and non-gelling system can be expressed as [149]:

$$n_m(t) \propto s(t)^{-2} f(m/s(t)), \quad (54)$$

where  $f(x)$  is a scaling function that depends on the sign of  $\mu$ . The  $f(x)$  decreases monotonically for kernels with  $\mu \geq 0$  (I and II class), whereas it is a bell-shaped function for  $\mu < 0$ .

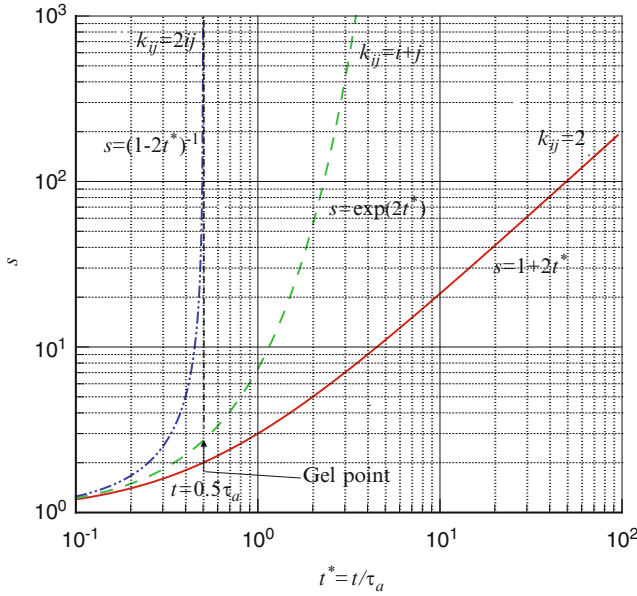


**Fig. 10** Mean cluster size  $s(t)$  versus dimensionless time  $t^* = t/\tau_a$  for different types of kernels. Arrow shows the gelling time,  $t_g = 0.5\tau_a$  for the product kernel,  $k_{ij} = 2ij$

The time dependence of mean cluster size  $s(t)$  at  $\lambda < 1$  follows:

$$s(t) \propto t^z, \quad (55)$$

at  $\lambda = 1$ , it follows:

$$s(t) \propto \exp(\alpha t), \quad (56)$$

and for gelling systems:

$$s(t) \propto (1 - t/t_g)^\beta. \quad (57)$$

Here,  $\alpha$  and  $\beta$  are constants and the following is a dynamic exponent:

$$z = 1/(1 - \lambda). \quad (58)$$

Note that continuous transition from  $z = 1$  ( $\lambda = 0$ ) to  $z = \infty$  ( $\lambda = 1$ ) corresponds to the transition from DLA to RLA model [150].

Figure 10 shows the examples of  $s$  versus  $t/\tau_a$  obtained from analytical solutions presented in Table 2 for constant ( $k_{ij} = 2$ ), sum ( $k_{ij} = i + j$ ), and product ( $k_{ij} = 2ij$ ) kernels. It is important that the three basic kernels can be used for an approximate description of the main features of DLA (Eq. 55), RLA (Eq. 56), and gelling (Eq. 57) models.

Finally, both theory and experiments have shown a universal long-term behavior of the cluster-size distribution  $n_m(t)$  for non-gelling systems,  $\lambda < 1$  [148, 149]:

$$\begin{aligned} n_m(t)/n_1(t) &\rightarrow \infty, & \mu < 1 \\ n_m(t) &\sim t^{-w} m^{-\tau}, & \mu < 0, w > 1, \tau < \lambda + 1 \\ n_m(t) &\sim t^{-w} m^{-\tau}, & \mu > 1, w = 1, \tau = \lambda + 1 \end{aligned} \quad (59)$$

where  $w$  and  $\tau$  are the scaling exponents.

To date, the dynamic scaling in heteroaggregation within the PBE approach was mainly tested for the simplified kernels. Practical applications of Eq. 51 for kernel estimation is restricted because of the absence of detailed relations for interactions of real particles with the fractal structure or rough surface.

The realistic kernels of different types were tested for a description of RLA aggregation [151–153]. The following two types of kernels:

$$k_{ij} = \frac{k_{ij}^{\text{Bf}}}{W_{ij}} (ij)^\lambda \quad (60)$$

and:

$$k_{ij} = \frac{k_{ij}^{\text{Bf}}}{W_{ij}} \frac{(ij)^\lambda}{1 + [(ij)^\lambda - 1]/W_{ij}}, \quad (61)$$

were used for comparison of the theory and experiments [151]. Here,  $k_{ij}^{\text{Bf}}$  is the Brownian kernel of fractal particles and  $W_{ij}$  is the stability ratio.

It was assumed that the stability ratio is constant in the course of aggregation,  $W_{ij} \approx W^{\text{in}}$ . The initial value,  $W^{\text{in}}$ , was experimentally determined for polymer latex particles in aqueous suspensions. The aggregation rate was measured at the very initial stage, where the presence of triplets was negligible [151]. The kernels in Eqs. 60, 62 were found to be appropriate for simulation of experimental results subject to proper tuning of the exponent  $\lambda$ . Moreover, the kernels in Eq. 62 were suitable for description of the continuous transition from DLA-like aggregation at  $W = 1$  to RLA-like aggregation at  $W \rightarrow \infty$  [152].

The Brownian dynamic simulations of aggregation between the oppositely charged particles were made using classical DLVO potential [111]. The results were compared with theoretical calculations using a twofold homogeneous kernel,  $k_{ij} \propto (i + j)^\lambda$ , where  $\lambda$  ( $\leq 0$ ) is the homogeneity parameter. The exponent  $z$  (see, Eq. 58) obtained from simulation was an increasing function of  $r/\lambda_D$ . The continuous transition from ballistic-like aggregation, at low  $r/\lambda_D$  ( $z < 1$ ), to DLA-like aggregation, at high  $r/\lambda_D$  ( $z = 1$ ), was observed. Most of the features of charge heteroaggregation kinetics obtained using Brownian dynamic simulation were well described by the PBE theory with dynamic exponent  $z$  estimated as  $\simeq 1/(1 - \lambda)$ .

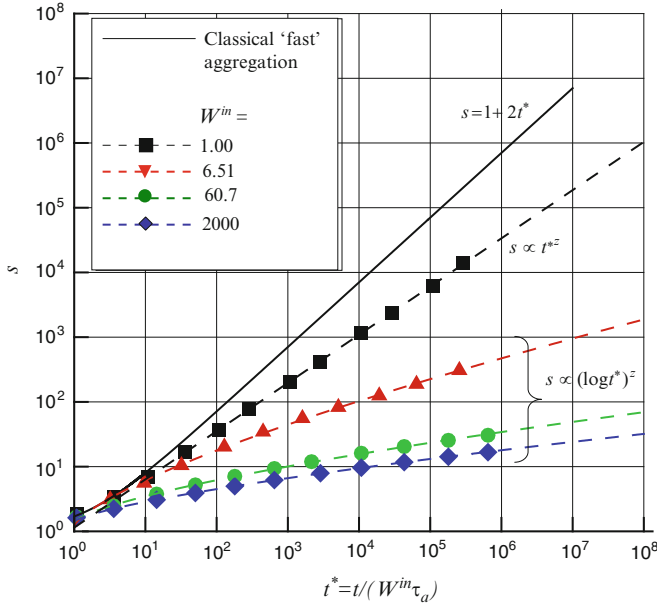


**Fig. 11** Mean particle size  $s$  versus dimensionless time  $t^* = t/W^{\text{in}}\tau_a$  for different initial values of stability ratios  $W^{\text{in}} = 1$ ,  $W^{\text{in}} = 6.51$  ( $\lambda_D = 1$  nm),  $W^{\text{in}} = 60.7$  ( $\lambda_D = 2$  nm), and  $W^{\text{in}} = 2,000$  ( $\lambda_D = 9$  nm). The *solid line* corresponds to the classical model of fast aggregation, where size dependence of the aggregate diffusion coefficient is neglected. *Dashed lines* are results of approximation by the power law ( $s \propto t^{*z}$ ,  $W^{\text{in}} = 1$ ), or logarithmic power law ( $s \propto (\log t^*)^z$ ,  $W^{\text{in}} > 1$ ). The simulations were done assuming  $A = 10^{-20}$  J and  $\zeta = 40$  mV. Compiled from published data [154]

Recently, computer simulations of the aggregation process of PEC nanoparticles were carried out [154]. The aggregation kinetics was studied accounting for the size dependence of the aggregate diffusion coefficient, classical DLVO potential for interactions between two unequal particles, and Fuchs stability ratio with hydrodynamic corrections. It was assumed that the value of stability factor  $W_{ij}$  is not constant and depends upon the size and charge of aggregating species. Figure 11 presents the calculated time dependencies of mean particle size  $s$  for different initial values of the stability ratio  $W^{\text{in}} = W_{ij}(t = 0)$ . The classical constant rate approximation results in overestimation of the mean size of a particle compared to the non-classical model of fast aggregation ( $W_{ij} = 1$ ) with the size-dependent diffusion coefficient. Note that both models follow the power law  $s(t)$  dependence (Eq. 55), but with different dynamic exponents,  $z = 1$  and  $z = 0.745 \pm 0.005$ , for the classical and non-classical models of fast aggregation, respectively (Fig. 11). The simulated data show a noticeable deviation of  $s(t)$  curves for slow aggregation ( $W^{\text{in}} > 1$ ) from the same curves for fast aggregation ( $W^{\text{in}} = 1$ ).



Moreover, analysis of data presented by Starchenko et al. [154] have shown that the universal logarithmic scaling:

$$s(t) \propto (\log t)^z, \quad (62)$$

with the same exponent  $z = 0.70 \pm 0.01$  was observed for all the studied values of  $W^{\text{in}} (>1)$ .

This result reflects a noticeable increase in  $W_{ij}$  stability ratios in the course of aggregation compared to the initial value  $W^{\text{in}}$ . The data demonstrate also that enhancement of the electrostatic repulsion, related to the increase in the Debye length  $\lambda_D$  or  $\zeta$  potential, results in a retardation of the growth. Good correspondence between theory and experiment was observed at small Debye length,  $\lambda_D < 3\text{--}5$  nm, in the so-called colloid regime. However, the effect of electrolyte on the PEC conformation became important at larger  $\lambda_D$  and simulation failed to describe experiments [154].

## 5 Conclusion

The study of aggregation has been intensively developed during the last 100 years and is relatively mature. However, aggregation is a very complex problem and this field still remains an open research area. Colloid stability is basically defined by interparticle forces of different origin and interaction length. The exact analytical expressions have not yet been obtained for many important contributions. Moreover, in suspensions of charged particles, the long-range and many-body effects, collective correlations between charges, and the effects of charges heterogeneously distributed on the surface of particles (so-called patchy surfaces [155]) may be particularly important. For polymeric systems, the emphasis should be directed towards the interaction between core-shell particles containing a compact core and covered by a charged soft shell. The theory and experiments show realization of the different morphologies of the aggregates, including compact, linear-like, branched, fractal, and mixed morphologies. However, the advantages of computer simulations are still restricted by relatively small and closed systems and, as a rule, the use of very primitive models for interparticle potentials. The theoretical understanding of aggregation kinetics is mainly based on original Smoluchowski theory (1917) and oversimplified assumptions about the size dependence of both the cluster diffusion coefficient and sticking probability. More complex analysis is required to account for the restructuring of aggregates, which can be particularly important for clusters with fractal morphology [156]. Finally, the aggregation processes in PEC nanoparticles are still far from being fully understood. For these systems, which behave as suspensions of core-shell particles, the impact of polyelectrolyte conformations on the final size of nanoparticles was revealed [154]. Future progress needs the range of experimentally studied types of polyions to be broadened and the development of more sophisticated theories in order to prepare aggregates of PEC particles with desired size and properties.

**Acknowledgements** The author appreciates the financial support from the National Academy of Sciences of Ukraine and Dr. N. S. Pivovarov for her help with the preparation of the manuscript.

## References

1. Mohanraj VYC (2006) Nanoparticles a review. *Trop J Pharm Res* 5(1):561–573
2. Hartig S, Greene R, Dikov M, Prokop A, Davidson J (2007) Multifunctional nanoparticulate polyelectrolyte complexes. *Pharmaceut Res* 24:2353–2369. doi:[10.1007/s11095-007-9459-1](https://doi.org/10.1007/s11095-007-9459-1)
3. Lankalapalli S, Kolapalli VRM (2009) Polyelectrolyte complexes: a review of their applicability in drug delivery technology. *Indian J Pharm Sci* 71(5):481–487. doi:[10.4103/0250-474X.58165](https://doi.org/10.4103/0250-474X.58165)
4. Muller M, Kesler B, Frohlich J, Poeschla S, Torger B (2011) Polyelectrolyte complex nanoparticles of poly(ethyleneimine) and poly(acrylic acid): preparation and applications. *Polymer* 52(2):762–778. doi:[10.3390/polym3020762](https://doi.org/10.3390/polym3020762)
5. Müller M, Reihs T, Ouyang W (2005) Preparation of monomodal polyelectrolyte complex nanoparticles of pdadmac/poly(maleic acid-alt- $\alpha$ -methylstyrene) by consecutive centrifugation. *Langmuir* 21(1):465–469
6. Dautzenberg H (2000) Light scattering studies on polyelectrolyte complexes. *Macromol Symp* 162:1–21
7. Panyam P, Labhasetwar V (2003) Biodegradable nanoparticles for drug and gene delivery to cells and tissue. *Adv Drug Deliv Rev* 55:329–347
8. Derjaguin BV, Landau L (1941) Theory of the stability of strongly charged lyophobic sols and of the adhesion of strongly charged particles in solutions of electrolytes. *Acta Phys Chim USSR* 14:633–662
9. Verwey EJW, Overbeek JTG (1948) Theory of the stability of lyophobic colloids. Elsevier, Amsterdam
10. Quemada D, Berli C (2002) Energy of interaction in colloids and its implications in rheological modeling. *Adv Colloid Interface Sci* 98(1):51–85. doi:[10.1016/S0001-8686\(01\)00093-8](https://doi.org/10.1016/S0001-8686(01)00093-8)
11. Eastman J (2010) Stability of charge-stabilised colloids. In: *Colloid science: principles, methods and applications*, 2nd edn. Wiley-Blackwell
12. Derjaguin BV (1934) Untersuchungen ueber die reibung und adhaesion IV. Theorie des anhaften kleiner teilchen. *Kolloid Z* 69:155–164
13. Israelachvili J (1991) Intermolecular and surface forces. Academic, New York
14. Shaw DJ (1992) Introduction to colloid and surface chemistry. Butterworth-Heinemann, Oxford
15. Mahanty J, Ninham B (1976) Dispersion forces. Academic, New York
16. Russel WB, Saville DA, Schowalter WR (1989) Colloidal dispersions. Cambridge University Press, New York
17. Malins A, Williams SR, Eggers J, Tanaka H, Royall CP (2011) The effect of inter-cluster interactions on the structure of colloidal clusters. *J Non-Cryst Solids* 357(2):760–766. doi:[10.1016/j.jnoncrysol.2010.08.021](https://doi.org/10.1016/j.jnoncrysol.2010.08.021)
18. dos Santos AP, Diehl A, Levin Y (2009) Electrostatic correlations in colloidal suspensions: density profiles and effective charges beyond the Poisson-Boltzmann theory. *J Chem Phys* 130:124110
19. Hogg R, Healy TW, Fuerstenau DW (1966) Mutual coagulation of colloidal dispersions. *Trans Faraday Soc* 62:1638–1651. doi:[10.1039/TF9666201638](https://doi.org/10.1039/TF9666201638)
20. Ohshima H, Healy TW, White LR (1982) Improvement on the Hogg-Healy-Fuerstenau formulas for the interaction of dissimilar double layers: I. Second and third approximations for moderate potentials. *J Colloid Interface Sci* 89(2):484–493. doi:[10.1016/0021-9797\(82\)90199-0](https://doi.org/10.1016/0021-9797(82)90199-0)

21. Elimelech M, Gregory J, Jia XWR (1995) Particle deposition and aggregation – measurement, modelling and simulation. Elsevier, Amsterdam
22. Boroudjerdi H, Kim YW, Naji A, Netz R, Schlagberger X, Serr A (2005) Statics and dynamics of strongly charged soft matter. *Phys Rep* 416(3–4):129–199. doi:[10.1016/j.physrep.2005.06.006](https://doi.org/10.1016/j.physrep.2005.06.006)
23. Kékicheff P, Spalla O (1995) Long-range electrostatic attraction between similar, charge-neutral walls. *Phys Rev Lett* 75:1851–1854. doi:[10.1103/PhysRevLett.75.1851](https://doi.org/10.1103/PhysRevLett.75.1851)
24. Kjellander R (1996) Ion-ion correlations and effective charges in electrolyte and macroion systems. *Ber Bunsen Phys Chem* 100(6):894–904. doi:[10.1002/bbpc.19961000635](https://doi.org/10.1002/bbpc.19961000635)
25. Larsen AE, Grier DG (1997) Like-charge attractions in metastable colloidal crystallites. *Nature* 385:230–233
26. Levin Y (2002) Electrostatic correlations: from plasma to biology. *Rep Prog Phys* 65:1577–1632
27. Bohinc K, Zelko J, Sunil Kumar PB, Iglic A, Kralj-Iglic V (2009) Attraction of like-charged surfaces mediated by spheroidal nanoparticles with spatially distributed electric charge: theory and simulation. In: *Advances in planar lipid bilayers and liposomes*, vol 9. Academic, Burlington
28. Vlachy V (1999) Ionic effects beyond Poisson-Boltzmann theory. *Annu Rev Phys Chem* 50:145–165
29. Shklovskii BI (1999) Screening of a macroion by multivalent ions: correlation-induced inversion of charge. *Phys Rev E* 60:5802–5811. doi:[10.1103/PhysRevE.60.5802](https://doi.org/10.1103/PhysRevE.60.5802)
30. Patra M, Patriarca M, Karttunen M (2003) Stability of charge inversion, thomson problem, and application to electrophoresis. *Phys Rev E* 67:031402. doi:[10.1103/PhysRevE.67.031402](https://doi.org/10.1103/PhysRevE.67.031402)
31. Levin Y (1999) When do like charges attract? *Physica A* 432:432–439
32. Levin Y (2005) Strange electrostatics in physics, chemistry, and biology. *Physica A* 352(1): 43–52. doi:[10.1016/j.physa.2004.12.033](https://doi.org/10.1016/j.physa.2004.12.033)
33. Trizac E, Raimbault JL (1999) Long-range electrostatic interactions between like-charged colloids: steric and confinement effects. *Phys Rev* 60:6530–6533
34. Kirkwood JG, Shumaker JB (1952) Forces between protein molecules in solution arising from fluctuations in proton charge and configuration. *Proc Natl Acad Sci USA* 38:863–871
35. Grønbech-Jensen N, Mashl RJ, Bruinsma RF, Gelbart WM (1997) Counterion-induced attraction between rigid polyelectrolytes. *Phys Rev Lett* 78:2477–2480. doi:[10.1103/PhysRevLett.78.2477](https://doi.org/10.1103/PhysRevLett.78.2477)
36. Belloni L, Spalla O (1997) Attraction of electrostatic origin between colloids. *J Chem Phys* 107(2):465–480. doi:[10.1063/1.474408](https://doi.org/10.1063/1.474408)
37. Podgornik R, Parsegian VA (1998) Charge-fluctuation forces between rodlike polyelectrolytes: pairwise summability reexamined. *Phys Rev Lett* 80:1560–1563. doi:[10.1103/PhysRevLett.80.1560](https://doi.org/10.1103/PhysRevLett.80.1560)
38. Squires TM, Brenner MP (2000) Like-charge attraction and hydrodynamic interaction. *Phys Rev Lett* 85:4976–4979. doi:[10.1103/PhysRevLett.85.4976](https://doi.org/10.1103/PhysRevLett.85.4976)
39. Allahyarov E, D’Amico I, Löwen H (1998) Attraction between like-charged macroions by coulomb depletion. *Phys Rev Lett* 81:1334–1337. doi:[10.1103/PhysRevLett.81.1334](https://doi.org/10.1103/PhysRevLett.81.1334)
40. Manning GS (1969) Limiting laws and counterion condensation in polyelectrolyte solutions I. Colligative properties. *J Chem Phys* 51(3):924–933. doi:[10.1063/1.1672157](https://doi.org/10.1063/1.1672157)
41. Arenzon J, Stilck J, Levin Y (1999) Simple model for attraction between like-charged polyions. *Eur Phys J B* 12:79–82
42. Tokuyama M (1998) Theory of slow dynamics in highly charged colloidal suspensions. *Phys Rev E* 58:R2729–R2732. doi:[10.1103/PhysRevE.58.R2729](https://doi.org/10.1103/PhysRevE.58.R2729)
43. Tokuyama M (1999) Effective forces between macroions in highly charged colloidal suspensions. *Phys Rev E* 59:R2550–R2553. doi:[10.1103/PhysRevE.59.R2550](https://doi.org/10.1103/PhysRevE.59.R2550)
44. Terada Y, Tokuyama M (2004) Novel liquid- and crystal-droplet phases on highly charged colloidal suspensions. *Physica A* 334(3–4):327–334. doi:[10.1016/j.physa.2003.10.078](https://doi.org/10.1016/j.physa.2003.10.078)
45. Fitch RM (1997) *Polymer colloids*. Academic, New York

46. Velegol D, Thwar PK (2001) Analytical model for the effect of surface charge nonuniformity on colloidal interactions. *Langmuir* 17:7687–7693. doi:[10.1021/la010634z](https://doi.org/10.1021/la010634z)
47. Czarnecki J (1985) The effects of surface inhomogeneities on the interactions in colloidal systems and colloid stability. *Adv Colloid Interface Sci* 24:283–319. doi:[10.1016/0001-8686\(85\)80035-X](https://doi.org/10.1016/0001-8686(85)80035-X)
48. Grant M, Saville D (1995) Electrostatic interactions between a nonuniformly charged sphere and a charged surface. *J Colloid Interface Sci* 171(1):35–45. doi:[10.1006/jcis.1995.1148](https://doi.org/10.1006/jcis.1995.1148)
49. Stankovich J, Carnie SL (1999) Interactions between two spherical particles with nonuniform surface potentials: the linearized poissonboltzmann theory. *J Colloid Interface Sci* 216(2):329–347. doi:[10.1006/jcis.1999.6326](https://doi.org/10.1006/jcis.1999.6326)
50. Schowalter WR, Eidsath AB (2001) Brownian flocculation of polymer colloids in the presence of a secondary minimum. *Proc Natl Acad Sci USA* 98:3644–3651. doi:[10.1073/pnas.061028498](https://doi.org/10.1073/pnas.061028498)
51. Podgornik R, Harries D, DeRouchey J, Strey HH, Parsegian VA (2008) Interactions in macromolecular complexes used as nonviral vectors for gene delivery. In: *Gene and cell therapy: therapeutic mechanisms and strategies*. CRC, Burlington
52. Morales V, Anta JA, Lago S (2003) Integral equation prediction of reversible coagulation in charged colloidal suspensions. *Langmuir* 19:475–482
53. de Gennes P (1981) Polymer solutions near an interface. 1. Adsorption and depletion layers. *Macromolecules* 14:1637–1644
54. de Gennes P (1982) Polymer solutions near an interface. 2. Interaction between two plates carrying adsorbed polymer layers. *Macromolecules* 15:492–500
55. Runkana V, Somasundaran P (2007) Mathematical modeling of coagulation and flocculation of colloidal suspensions incorporating the influence of surface forces. In: *Colloid stability and application in pharmacy*. Colloid and interface science series, vol 3. Wiley-VCH, Weinheim
56. Runkana V, Somasundaran P, Kapur P (2006) A population balance model for flocculation of colloidal suspensions by polymer bridging. *Chem Eng Sci* 61:182–191
57. Somasundaran P, Runkana V (2009) Aggregation of colloids: recent developments in population balance modeling. In: *Highlights in colloid science*. Wiley-VCH, Weinheim
58. Grier DG, Behrens SH (2001) Interactions in colloidal suspensions: electrostatics, hydrodynamics and their interplay. In: *Electrostatic effects in biophysics and soft matter*. Kluwer, Dordrecht
59. Derjaguin B, Muller V (1967) Slow coagulation of hydrophobic colloids. *Dokl Akad Nauk SSSR* 176:738–741
60. Spielman LA (1970) Viscous interactions in brownian coagulation. *J Colloid Interface Sci* 33(4):562–571. doi:[10.1016/0021-9797\(70\)90008-1](https://doi.org/10.1016/0021-9797(70)90008-1)
61. Brenner H (1961) The slow motion of a sphere through a viscous fluid towards a plane surface. *Chem Eng Sci* 16(34):242–251. doi:[10.1016/0009-2509\(61\)80035-3](https://doi.org/10.1016/0009-2509(61)80035-3)
62. Honig E, Roebersen G, Wiersema P (1971) Effect of hydrodynamic interaction on the coagulation rate of hydrophobic colloids. *J Colloid Interface Sci* 36(1):97–109. doi:[10.1016/0021-9797\(71\)90245-1](https://doi.org/10.1016/0021-9797(71)90245-1)
63. Kovalchuk N, Starov V (2011) Aggregation in colloidal suspensions: effect of colloidal forces and hydrodynamic interactions. *Adv Colloid Interface Sci*. doi:[10.1016/j.cis.2011.05.009](https://doi.org/10.1016/j.cis.2011.05.009)
64. Cao X, Cummins H, Morris J (2012) Hydrodynamic and interparticle potential effects on aggregation of colloidal particles. *J Colloid Interface Sci* 368(1):86–96. doi:[10.1016/j.jcis.2011.11.050](https://doi.org/10.1016/j.jcis.2011.11.050)
65. Furukawa A, Tanaka H (2010) Key role of hydrodynamic interactions in colloidal gelation. *Phys Rev Lett* 104:245702. doi:[10.1103/PhysRevLett.104.245702](https://doi.org/10.1103/PhysRevLett.104.245702)
66. Riese DO, Wegdam GH, Vos WL, Sprik R, Fenistein D, Bongaerts JH, Grübel G (2000) Effective screening of hydrodynamic interactions in charged colloidal suspensions. *Phys Rev Lett* 85(25):5460–5464

67. Muthukumar M (1997) Dynamics of polyelectrolyte solutions. *J Chem Phys* 107 (7):2619–2635. doi:[10.1063/1.474573](https://doi.org/10.1063/1.474573)
68. Muthukumar M (2005) Polyelectrolyte dynamics. In: Rice SA (ed) *Advances in chemical physics*, vol 131. Wiley, Hoboken
69. Arunachalam V, Marlow WH, Lu JX (1998) Development of a picture of the van der Waals interaction energy between clusters of nanometer-range particles. *Phys Rev E* 58:3451–3457
70. Babick F, Schiel K, Stintz M (2011) Van-der-Waals interaction between two fractal aggregates. *Adv Powder Technol* 22(2):220–225. doi:[10.1016/j.appt.2010.11.014](https://doi.org/10.1016/j.appt.2010.11.014)
71. Schiesl K, Babick F, Stintz M (2012) Calculation of double layer interaction between colloidal aggregates. *Adv Powder Technol* 23(2):139–147. doi:[10.1016/j.appt.2011.01.005](https://doi.org/10.1016/j.appt.2011.01.005)
72. Vicsek T (1992) *Fractal growth phenomena*. World Scientific, Singapore
73. Smoluchowski M (1917) Über brownische molekularebewegung unter einwirkung auserer kraefte und deren zusammenhang mit der verallgemeinerten diffusions- gleichung. *Ann Phys-Leipzig* 48:1103–1112
74. Meakin P (1999) A historical introduction to computer models for fractal aggregates. *J Sol-gel Sci Technol* 15:97–117
75. Witten TA, Sander LM (1981) Diffusion-limited aggregation, a kinetic critical phenomenon. *Phys Rev Lett* 47:1400–1403
76. Sutherland D (1966) Comment on Vold’s simulation of floc formation. *J Colloid Interface Sci* 22:300
77. Sutherland DN (1967) A theoretical model of floc structure. *J Colloid Interface Sci* 25:373–380
78. Vold M (1963) Computer simulation of floe formation in a colloidal suspension. *J Colloid Sci* 18:684–695
79. Eden M (1961) A two-dimensional growth process. In: *Proceedings of the Fourth Berkeley Symposium on Mathematics, Statistics and Probability*, vol 4: *Biology and Problems of Health*. University of California Press, Berkeley
80. Jullien R, Botet R (1987) *Aggregation and fractal aggregation*. World Scientific, Singapore
81. Aubert C, Cannell DS (1986) Restructuring of colloidal silica aggregates. *Phys Rev Lett* 56:738–741. doi:[10.1103/PhysRevLett.56.738](https://doi.org/10.1103/PhysRevLett.56.738)
82. Liu J, Shih WY, Sarikaya M, Aksay IA (1990) Fractal colloidal aggregates with finite interparticle interactions: energy dependence of the fractal dimension. *Phys Rev A* 41:3206–3213. doi:[10.1103/PhysRevA.41.3206](https://doi.org/10.1103/PhysRevA.41.3206)
83. Jia Z, Wu H, Morbidelli M (2007) Thermal restructuring of fractal clusters: the case of a strawberry-like core-shell polymer colloid. *Langmuir* 23:5713–5721. doi:[10.1021/la063254s](https://doi.org/10.1021/la063254s)
84. Jullien R, Meakin P (1989) Simple models for the restructuring of three-dimensional ballistic aggregates. *J Colloid Interface Sci* 127(1):265–272. doi:[10.1016/0021-9797\(89\)90027-1](https://doi.org/10.1016/0021-9797(89)90027-1)
85. Shih WY, Aksay IA, Kikuchi R (1987) Reversible-growth model: cluster-cluster aggregation with finite binding energies. *Phys Rev A* 36:5015–5019. doi:[10.1103/PhysRevA.36.5015](https://doi.org/10.1103/PhysRevA.36.5015)
86. Rioux C, Slobodrian RJ (2012) Experimental discrimination of electrostatic and magnetic forces in particle-particle aggregation. *Adv Space Res* 49(10):1408–1414
87. Groenewold J, Kegel WK (2004) Colloidal cluster phases, gelation and nuclear matter. *J Phys Condens Matter* 16:S4877–S4886
88. Sciortino F, Mossa S, Zaccarelli E, Tartaglia P (2004) Equilibrium cluster phases and low-density arrested disordered states: the role of short-range attraction and long-range repulsion. *Phys Rev Lett* 93:055701
89. Rayleigh L (1882) On the equilibrium of liquid conducting masses charged with electricity. *Philos Mag* 14:184–186
90. Smirnov BM (2006) *Cluster processes in gases and plasmas. Distributions, structures, phenomena, kinetics of atomic systems*. Wiley-VCH, Weinheim
91. Weizsacker CFV (1935) Zur theorie der kernmassen. *Z Phys* 96:431–458
92. Lu PJ, Conrad JC, Wyss HM, Schofield AB, Weitz DA (2006) Fluids of clusters in attractive colloids. *Phys Rev Lett* 96:028306. doi:[10.1103/PhysRevLett.96.028306](https://doi.org/10.1103/PhysRevLett.96.028306)

93. Lu PJ, Zaccarelli E, Ciulla F, Schofield AB, Sciortino F, Weitz DA (2008) Gelation of particles with short-range attraction. *Nature* 453:499–503. doi:[10.1038/nature06931](https://doi.org/10.1038/nature06931)
94. de Gennes P, Pincus P, Velasco R, Brochard F (1976) Remarks on polyelectrolyte conformation. *J Phys-Paris* 37(12):1461–1473
95. Brender C, Danino M, Shatz S (1999) Fractals in Monte Carlo simulations of a short polyelectrolyte. *J Phys A Math Gen* 32(2):235
96. Fernandez-Toledano JC, Moncho-Jorda A, Martinez-Lopez F, Gonzalez AE, Hidalgo-Alvarez R (2007) Two-dimensional colloidal aggregation mediated by the range of repulsive interactions. *Phys Rev E* 75:041408. doi:[10.1103/PhysRevE.75.041408](https://doi.org/10.1103/PhysRevE.75.041408)
97. Mossa S, Sciortino F, Tartaglia P, Zaccarelli E (2004) Ground-state clusters for short-range attractive and long-range repulsive potentials. *Langmuir* 20(24):10756–10763. doi:[10.1021/la048554t](https://doi.org/10.1021/la048554t)
98. Sciortino F, Tartaglia P, Zaccarelli E (2005) One-dimensional cluster growth and branching gels in colloidal systems with short-range depletion attraction and screened electrostatic repulsion. *J Phys Chem B* 109(46):21942–21953. doi:[10.1021/jp052683g](https://doi.org/10.1021/jp052683g)
99. Chakrabarty RK, Moosmuller H, Garro MA, Arnott WP, Slowik JG, Cross ES, Jeong-Ho Han PD, Onasch TB, Worsnop DR (2008) Morphology based particle segregation by electrostatic charge. *J Aerosol Sci* 39(9):785–792
100. Block A, van Blah W, Schellnhuber HJ (1991) Aggregation by attractive particle-cluster interaction. *J Phys A Math Gen* 24:L1037–L1044
101. Indiveri G, Scalas E, Levi A, Gliozzi A (1999) Morphologies in two-dimensional growth with attractive long-range interactions. *Physica A* 273(3–4):217–230. doi:[10.1016/S0378-4371\(99\)00231-9](https://doi.org/10.1016/S0378-4371(99)00231-9)
102. Meakin P (1990) The effects of attractive and repulsive interactions on three-dimensional reaction-limited aggregation. *J Colloid Interface Sci* 134(1):235–244. doi:[10.1016/0021-9797\(90\)90271-O](https://doi.org/10.1016/0021-9797(90)90271-O)
103. Meakin P, Muthukumar M (1989) The effects of attractive and repulsive interaction on two-dimensional reaction-limited aggregation. *J Chem Phys* 91(5):3212–3221. doi:[10.1063/1.456942](https://doi.org/10.1063/1.456942)
104. Indiveri G, Levi A, Gliozzi A, Scalas E (1996) Cluster growth with long-range interactions. *Thin Solid Films* 284–285:106–109
105. Ivanenko Y, Lebovka N, Vygornitskii N (1999) Eden growth model for aggregation of charged particles. *Eur Phys J B* 11:469–480
106. Lebovka NI, Ivanenko YV, Vygornitskii NV (1998) Deterministic eden model of charged-particles aggregation. *Europhys Lett* 41(1):19
107. Pinchuk AO, Kalsin AM, Kowalczyk B, Schatz GC, Grzybowski BA (2007) Modeling of electrodynamic interactions between metal nanoparticles aggregated by electrostatic interactions into closely-packed clusters. *J Phys Chem C* 111(32):11816–11822. doi:[10.1021/jp073403v](https://doi.org/10.1021/jp073403v)
108. Zhang R, Shklovskii B (2005) Phase diagram of solution of oppositely charged polyelectrolytes. *Physica A* 352(1):216–238. doi:[10.1016/j.physa.2004.12.037](https://doi.org/10.1016/j.physa.2004.12.037)
109. Harnau L, Hansen JP (2002) Colloid aggregation induced by oppositely charged polyions. *J Chem Phys* 116(20):9051–9057. doi:[10.1063/1.1471550](https://doi.org/10.1063/1.1471550)
110. Puertas A, Fernandez-Barbero A, De las Nieves F (2000) Aggregation between oppositely charged colloidal particles. In: Buckin V (ed) *Trends in colloid and interface science XIV. Progress in colloid and polymer science*, vol 115. Springer, Berlin, pp 55–58
111. Puertas A, Fernandez-Barbero A, de las Nieves F (2002) Kinetics of colloidal heteroaggregation. *Physica A* 304(34):340–354. doi:[10.1016/S0378-4371\(01\)00564-7](https://doi.org/10.1016/S0378-4371(01)00564-7)
112. Kim AY, Hauch KD, Berg JC, Martin JE, Anderson RA (2003) Linear chains and chain-like fractals from electrostatic heteroaggregation. *J Colloid Interface Sci* 260(1):149–159. doi:[10.1016/S0021-9797\(03\)00033-X](https://doi.org/10.1016/S0021-9797(03)00033-X)

113. Cerbelaud M, Videcoq A, Abelard P, Pagnoux C, Rossignol F, Ferrando R (2008) Heteroaggregation between  $\text{Al}_2\text{O}_3$  submicrometer particles and  $\text{SiO}_2$  nanoparticles: experiment and simulation. *Langmuir* 24(7):3001–3008. doi:[10.1021/la702104u](https://doi.org/10.1021/la702104u)
114. Cerbelaud M, Videcoq A, Abelard P, Ferrando R (2009) Simulation of the heteroagglomeration between highly size-asymmetric ceramic particles. *J Colloid Interface Sci* 332(2):360–365. doi:[10.1016/j.jcis.2008.11.063](https://doi.org/10.1016/j.jcis.2008.11.063)
115. Piechowiak MA, Videcoq A, Ferrando R, Bochicchio D, Pagnoux C, Rossignol F (2012) Aggregation kinetics and gel formation in modestly concentrated suspensions of oppositely charged model ceramic colloids: a numerical study. *Phys Chem Chem Phys* 14:1431–1439. doi:[10.1039/C1CP22980J](https://doi.org/10.1039/C1CP22980J)
116. Castelnovo M, Sens P, Joanny JF (2000) Charge distribution on annealed polyelectrolytes. *Eur Phys J E* 1:115–125
117. Coslovich D, Hansen J, Kahl G (2011) Ultrasoft primitive model of polyionic solutions: structure, aggregation, and dynamics. *J Chem Phys* 134(24):244514 (15 pages), [www.scopus.com](http://www.scopus.com)
118. Coslovich D, Hansen JP, Kahl G (2011) Clustering, conductor-insulator transition and phase separation of an ultrasoft model of electrolytes. *Soft Matter* 7:1690–1693. doi:[10.1039/C0SM01090A](https://doi.org/10.1039/C0SM01090A)
119. Lee J, Popov YO, Fredrickson GH (2008) Complex coacervation: a field theoretic simulation study of polyelectrolyte complexation. *J Chem Phys* 128(22):224908. doi:[10.1063/1.2936834](https://doi.org/10.1063/1.2936834)
120. Rydén J, Ullner M, Linse P (2005) Monte Carlo simulations of oppositely charged macroions in solution. *J Chem Phys* 123(3):034909. doi:[10.1063/1.1949191](https://doi.org/10.1063/1.1949191)
121. Zito T, Seidela C (2002) Equilibrium charge distribution on annealed polyelectrolytes. *Eur Phys J E* 8:339–346
122. Buchhammer HM, Mende M, Oelmann M (2003) Formation of mono-sized polyelectrolyte complex dispersions: effects of polymer structure, concentration and mixing conditions. *Colloids Surf A* 218(1):151–159. doi:[10.1016/S0927-7757\(02\)00582-4](https://doi.org/10.1016/S0927-7757(02)00582-4)
123. Buchhammer HM, Mende M, Oelmann M (2004) Preparation of monodisperse polyelectrolyte complex nanoparticles in dilute aqueous solution. In: Tauer K (ed) *Aqueous polymer dispersions. Progress in colloid and polymer science*, vol 124. Springer, Berlin, pp 98–102
124. Dobrynin AV (2008) Theory and simulations of charged polymers: from solution properties to polymeric nanomaterials. *Curr Opin Colloid Interface Sci* 13(6):376–388. doi:[10.1016/j.cocis.2008.03.006](https://doi.org/10.1016/j.cocis.2008.03.006)
125. Oskolkov NN, Potemkin II (2007) Complexation in asymmetric solutions of oppositely charged polyelectrolytes: phase diagram. *Macromolecules* 40(23):8423–8429. doi:[10.1021/ma0709304](https://doi.org/10.1021/ma0709304)
126. Popov YO, Lee J, Fredrickson G (2007) Field-theoretic simulations of polyelectrolyte complexation. *J Polym Sci Pol Phys* 45:3223–3230
127. Dalakoglou G, Karatasos K, Lyulin S, Lyulin A (2008) Brownian dynamics simulations of complexes of hyperbranched polymers with linear polyelectrolytes: effects of the strength of electrostatic interactions on static properties. *Mat Sci Eng B-Solid* 152(1–3):114–118. doi:[10.1016/j.mseb.2008.06.012](https://doi.org/10.1016/j.mseb.2008.06.012)
128. Skepo M, Linse P (2003) Complexation, phase separation, and redissolution in polyelectrolyte-macroion solutions. *Macromolecules* 36:508–519
129. Feng J, Ruckenstein E (2003) Monte Carlo simulation of polyampholyte-nanoparticle complexation. *Polymer* 44(10):3141–3150. doi:[10.1016/S0032-3861\(03\)00208-8](https://doi.org/10.1016/S0032-3861(03)00208-8)
130. Ulrich S, Seijo M, Carnal F, Stoll S (2011) Formation of complexes between nanoparticles and weak polyampholyte chains. Monte Carlo simulations. *Macromolecules* 44:1661–1670
131. Sennato S, Truzzolillo D, Bordi F, Sciortino F, Cametti C (2009) Colloidal particle aggregates induced by particle surface charge heterogeneity. *Colloids Surf A* 343(1–3):34–42. doi:[10.1016/j.colsurfa.2009.01.026](https://doi.org/10.1016/j.colsurfa.2009.01.026)
132. Jeon J, Dobrynin AV (2005) Molecular dynamics simulations of polyampholyte-polyelectrolyte complexes in solutions. *Macromolecules* 38:5300–5312



133. Xu Y, Feng J, Liu H, Hu Y, Jiang J (2007) Molecular dynamics simulation of polyelectrolyte with oppositely charged monomeric and dimeric surfactants. *Mol Simul* 33(3):261–268. doi:[10.1080/08927020601158679](https://doi.org/10.1080/08927020601158679)
134. Jullien R, Botet R, Mors PM (1987) Computer simulations of cluster-cluster aggregation. *Faraday Discuss Chem Soc* 83:125–137. doi:[10.1039/DC9878300125](https://doi.org/10.1039/DC9878300125)
135. Mors PM, Botet R, Jullien R (1987) Cluster-cluster aggregation with dipolar interactions. *J Phys A Math Gen* 20:L975
136. Pastor-Satorras R, Rubi JM (1995) Particle-cluster aggregation with dipolar interactions. *Phys Rev E* 51:5994–6003
137. Pastor-Satorras R, Rubi R (1998) Fractal properties of cluster of colloidal magnetic particles. *Prog Colloid Polym Sci* 110:29–33
138. Pastor-Satorras R, Rubi J (2000) Dipolar interactions induced order in assemblies of magnetic particles. *J Magn Magn Mater* 221:124–131
139. Family F (1985) *Kinetics of aggregation and gelation*. Elsevier, Amsterdam
140. Meakin P (1992) *Aggregation kinetics*. *Phys Scripta* 46(4):295
141. Meakin P (1998) *Fractals, scaling and growth far from equilibrium*. Cambridge University Press, Cambridge
142. Fuchs N (1934) Ueber die stabilitat und aufladung der aerosole. *Z Phys* 89:736–743
143. Reerink H, Overbeek JTG (1954) The rate of coagulation as a measure of the stability of silver iodide sols. *Faraday Discuss Chem Soc* 18:74–84
144. Leyvraz F (2003) Scaling theory and exactly solved models in the kinetics of irreversible aggregation. *Phys Rep* 383:95–212
145. McLeod JB (1962) On an infinite set of non-linear differential equations. *Q J Math* 13:119–128
146. Melzak ZA (1953) The effects of coalescence in certain collision processes. *Q J Mech Appl Math* 11:231–234
147. Gmachowski L (2000) Estimation of the dynamic size of fractal aggregates. *Colloids Surf A* 170(23):209–216. doi:[10.1016/S0927-7757\(99\)00532-4](https://doi.org/10.1016/S0927-7757(99)00532-4)
148. Zift RM, McGrady ED, Meakin P (1985) On the validity of Smoluchowski's equation for cluster-cluster aggregation kinetics. *J Chem Phys* 82:5269–5274
149. Fernandez-Barbero A, Cabrero-Vilchez M, Martinez-Garcia R, Hidalgo-Alvarez R (1996) Effect of the particle surface charge density on the colloidal aggregation mechanism. *Phys Rev E* 53:4981–4989. doi:[10.1103/PhysRevE.53.4981](https://doi.org/10.1103/PhysRevE.53.4981)
150. Asnaghi D, Carpineti M, Giglio M, Sozzi M (1992) Coagulation kinetics and aggregate morphology in the intermediate regimes between diffusion-limited and reaction-limited cluster aggregation. *Phys Rev A* 45:1018–1023. doi:[10.1103/PhysRevA.45.1018](https://doi.org/10.1103/PhysRevA.45.1018)
151. Lattuada M, Sandkuhler P, Wu H, Sefcik J, Morbidelli M (2003) Aggregation kinetics of polymer colloids in reaction limited regime: experiments and simulations. *Adv Colloid Interface Sci* 103:33–56
152. Odriozola G, Moncho-Jorda A, Schmitt A, Callejas-Fernandez J, Martinez-Garcia R, Hidalgo-Alvarez R (2001) A probabilistic aggregation kernel for the computer-simulated transition from DLCA to RLCA. *Europhys Lett* 53:797803
153. Runkana V, Somasundaran P, Kapur PC (2005) Reaction-limited aggregation in presence of short-range structural forces. *AIChE J* 51:1233–1245
154. Starchenko V, Muller M, Lebovka N (2008) Growth of polyelectrolyte complex nanoparticles: computer simulations and experiments. *J Phys Chem C* 112:8863–8869
155. Bianchi E, Blaak R, Likos CN (2011) Patchy colloids: state of the art and perspectives. *Phys Chem Chem Phys* 13:6397–6410. doi:[10.1039/C0CP02296A](https://doi.org/10.1039/C0CP02296A)
156. Gruy F (2011) Population balance for aggregation coupled with morphology changes. *Colloids Surf A* 374(13):69–76. doi:[10.1016/j.colsurfa.2010.11.010](https://doi.org/10.1016/j.colsurfa.2010.11.010)



Polyelectrolyte Complexes in the Dispersed and Solid  
State I

Principles and Theory

Müller, M. (Ed.)

2014, VII, 229 p. 70 illus., 4 illus. in color., Hardcover

ISBN: 978-3-642-40733-8